iScience

CellPress
OPEN ACCESS

Article

Distinct hypoxia-induced translational profiles of embryonic and adult-derived macrophages

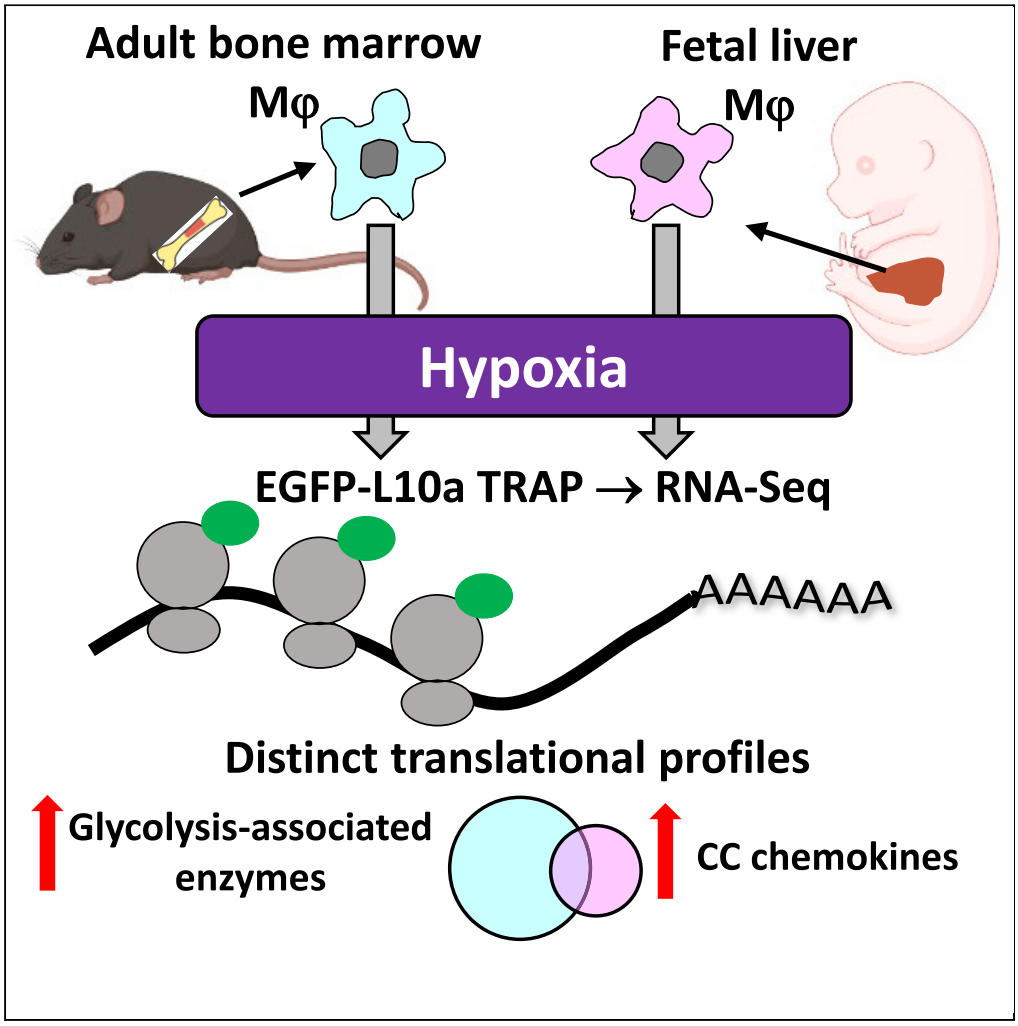

Nicholas S. Wilcox, Timur O. Yarovinsky, Prakruti Pandya, ..., Stefania Nicoli, Karen K. Hirschi, Jeffrey R. Bender

jeffrey.bender@yale.edu

Highlights

Hypoxia alters profiles of total and translated poly(A) RNA in BMDM and FLDM

Hypoxia regulates different immune and metabolic regulators in BMDM and FLDM

RNA-binding protein HuR modifies macrophage responses to hypoxia and tissue injury

Wilcox et al., iScience *26*, 107985
December 15, 2023 © 2023
https://doi.org/10.1016/j.isci.2023.107985

iScience

CellPress
OPEN ACCESS

Article

Distinct hypoxia-induced translational profiles of embryonic and adult-derived macrophages

Nicholas S. Wilcox,[1,2,4,7] Timur O. Yarovinsky,[1,2,7] Prakruti Pandya,[1,2] Vinod S. Ramgolam,[1,2] Albertomaria Moro,[1,3,5] Yinyu Wu,[1,3] Stefania Nicoli,[1,3] Karen K. Hirschi,[1,3,6] and Jeffrey R. Bender[1,2,8,*]

SUMMARY

Tissue resident macrophages are largely of embryonic (fetal liver) origin and long-lived, while bone marrow–derived macrophages (BMDM) are recruited following an acute perturbation, such as hypoxia in the setting of myocardial ischemia. Prior transcriptome analyses identified BMDM and fetal liver–derived macrophage (FLDM) differences at the RNA expression level. Posttranscriptional regulation determining mRNA stability and translation rate may override transcriptional signals in response to hypoxia. We profiled differentially regulated BMDM and FLDM transcripts in response to hypoxia at the level of mRNA translation. Using a translating ribosome affinity purification (TRAP) assay and RNA-seq, we identified non-overlapping transcripts with increased translation rate in BMDM (Ly6e, vimentin, PF4) and FLDM (Ccl7, Ccl2) after hypoxia. We further identified hypoxia-induced transcripts within these subsets that are regulated by the RNA-binding protein HuR. These findings define translational differences in macrophage subset gene expression programs, highlighting potential therapeutic targets in ischemic myocardium.

INTRODUCTION

Macrophages populate all tissues and exert multiple functions to maintain homeostasis in response to environmental changes.[1] Embryonic macrophages originating from the yolk sac or fetal liver populate most organs during early development and constitute the majority of tissue-resident macrophages. Fate mapping studies in mice reveal that more than 95% of cardiac- and lung-resident macrophages originate from fetal liver.[2,3] Under homeostatic conditions, tissue resident macrophages undergo self-renewal with little influx from the bone marrow.[4] However, organ injury or inflammation results in rapid recruitment of bone marrow–derived monocytes that differentiate into macrophages with overlapping and distinct roles in tissue repair, from those of tissue-resident cells.[2,3,5,6]

Reduced blood flow to organs (i.e., ischemia) decreases oxygen availability in target tissues while oxygen deprivation impairs oxidative phosphorylation in mitochondria and diminishes ATP production.[7,8] Energy starvation results in shutdown of general protein synthesis via mechanisms involving phosphorylation and inactivation of eukaryotic initiation factor-2α and eukaryotic translation elongation factor 2, and suppression of the mammalian target of rapamycin.[9,10] On the other hand, hypoxia-induced stabilization of hypoxia-inducible factor-1α (HIF-1α), followed by nuclear translocation and association with HIF-1β, leads to transcriptional activation of multiple genes involved in adaptation to hypoxic conditions.[11–13] Translation of specific transcripts under hypoxic conditions depends on binding of HIF-2α to the hypoxia response elements at the 3′UTR as well as a switch from the cap-dependent to -independent mRNA translation, initiated from the internal ribosome entry site (IRES).[14–16] Tissue-resident and newly recruited macrophages sense hypoxic conditions and rely on HIF-mediated transcriptional activation to promote angiogenesis and tissue repair.[17–20]

Posttranscriptional regulation of gene expression at the level of mRNA stability and translation may amplify or override transcriptional regulation and, as such, plays an important role in macrophage responses to hypoxia.[19,21] Multiple RNA-binding proteins, including HuR, PTB, TTP, and others, change mRNA turnover and translation rate by selectively binding to the 5′UTR or 3′UTR of the target mRNAs.[22] For example, HuR can stabilize macrophage transcripts regulated by HIF-1α, including vascular endothelial growth factor A (Vegf) and matrix metalloproteinase-9 (Mmp9), which modulate angiogenesis and tissue repair.[23] On the other hand, latent binding of HuR to the 5′UTR of

[1]Department of Internal Medicine, Section of Cardiovascular Medicine, Yale Cardiovascular Research Center, New Haven, CT USA
[2]Department of Immunobiology, and Yale University School of Medicine, New Haven, CT 06511, USA
[3]Department of Genetics, Yale University School of Medicine, New Haven, CT 06511, USA
[4]Present address: Hospital of the University of Pennsylvania, 3400 Spruce Street, Philadelphia, Pennsylvania, 19104, USA
[5]Present address: Department of Developmental Biology, Sloan Kettering Institute, 1275 York Ave, Box 252, New York, NY 10065, USA
[6]Present address: Department of Cell Biology, University of Virginia, Pinn Hall, 3rd Floor, 1340 Jefferson Park Ave, Charlottesville, VA 22903, USA
[7]These authors contributed equally
[8]Lead contact
*Correspondence: jeffrey.bender@yale.edu
https://doi.org/10.1016/j.isci.2023.107985

caspase-2, Bcl_{XL} and p27 mRNAs inhibits IRES-dependent translation from those transcripts.[24–26] Another level of posttranscriptional regulation complexity is added by microRNAs (miRNAs), which cause RNA degradation or translational arrest through binding to mRNA 3′-UTRs.[22] HuR can compete with miRNAs for binding to neighboring 3′-UTR sites, thereby conferring protection.[27,28] The attenuation of miRNA binding to transcripts in close proximity to HuR binding sites, and consequential miRNA targeting of transcripts regulating angiogenesis and macrophage/endothelial interactions, have been demonstrated.[29]

There are global and specific changes in macrophage mRNA translation in response to various stimuli, including hypoxia.[19,30–33] However, prior studies have either focused on bone marrow-derived macrophages (BMDM) or simply did not attempt to address the origin of macrophages. Considering the differences in the differentiation pathways and transcription programs between adult BMDM and embryonically derived macrophages, we hypothesized that BMDM and fetal liver–derived macrophages (FLDM) respond to hypoxia by changing translation of distinct subsets of mRNAs, some in an HuR-dependent manner. These differences might dictate dominant homeostatic and pathologic responses in a given tissue and form the basis for therapeutic targets.

To test our hypothesis, we differentiated macrophages from fetal liver and bone marrow of transgenic mice that express a codon optimized Cre recombinase (iCre) under the control of colony stimulating factor 1 receptor (Csfr1) promoter and, after Cre-mediated recombination, large ribosomal protein L10a fused to EGFP from the Rosa26 locus.[34,35] This approach enabled unbiased transcriptome wide assessment of the total and ribosome-occupied (i.e., translated) poly(A) RNA in BMDM and FLDM at baseline and after exposure to hypoxia using translating ribosome affinity purification (TRAP). This method has been used to estimate mRNA translation efficiency in many cell types and experimental systems.[32,36–38] As L10a-EGFP is included in the polysome fractions.[35,39,40] TRAP assay effectively measures ribosome occupancy for specific transcripts. A single workflow for RNA-seq analyses of total and translated poly(A) transcripts isolated from the same, homogeneous samples in culture enabled us to effectively measure translation efficiency defined as the ratio of translated to total poly(A). We found that BMDM, but not FLDM, respond to hypoxia primarily by upregulating translation of mRNAs encoding glycolytic enzymes. Furthermore, BMDM increased translation of multiple functionally diverse immune regulators, whereas FLDM increased translation of CC chemokines Ccl7 and Ccl2. Finally, by using conditional deletion of HuR in macrophages, we identified transcripts that were differentially regulated by this RNA-binding protein in the context of hypoxia.

RESULTS

BMDM and FLDM for translational profiling

To compare mRNA translation in macrophages of embryonic vs. adult origin, we expanded macrophages from fetal livers or adult bone marrow of $Csf1r^{iCre}Rosa26^{EGFP:L10a}$ mice in the presence of conditioned medium from L929 fibroblasts containing M-CSF for 6–7 days. More than 90% of the cells in culture were GFP+, indicating expression of EGFP-L10a, and more than 90% of GFP+ cells were positive for CD11b and F4/80, a marker for differentiated macrophages (Figure 1A). BMDM and FLDM cultures were similar morphologically with EGFP-L10a present in both the nucleus and cytoplasm (Figure 1B).

We exposed differentiated BMDM and FLDM to hypoxia (1% O_2, 5% CO_2, balanced with nitrogen) for 18 h and applied RNA-seq analyses to the total vs. translated poly(A) RNA pools isolated with translated ribosome affinity purification (TRAP). The results were expressed as transcripts per kilobase million (TPM) to determine abundance and translation for each mapped transcript. The numbers of unique mapped transcripts with TPM>0 in the total vs. translated poly(A) pools were similar: 13,883 vs. 11,735 in the BMDM samples and 11,651 vs. 10,624 in the FLDM samples. Total and translated poly(A) samples were predominantly protein-coding mRNAs, but also included some non-coding RNAs (miRNA and lncRNA) and mitochondria-encoded mRNA. The latter were highly abundant in the total RNA samples, reduced in the translated pools by ~50-fold (Figure S1).

The mRNAs encoding macrophage-specific markers Adgre1 (F4/80), Csf1r, CD14 and CD68 were highly abundant in total and translated RNA pools for both macrophage types under normoxic and hypoxic conditions (Figure 1C). At the whole transcriptome level, strong correlation was evident between abundance and translation of most transcripts in BMDM and FLDM under normoxic and hypoxic conditions ($p < 0.0001$) (Figure 1C). However, a number of transcripts were either under- or over-represented in the translated poly(A) relative to total poly(A) pools (Figure 1C).

Hypoxia-induced changes in the total poly(A) RNA transcriptome

RNA-seq analyses of the total poly(A) RNA showed weak correlation of hypoxia-induced changes between BMDM and FLDM (Figure 2A). Among the protein-coding transcripts, 15 were significantly upregulated and 8 were significantly downregulated in BMDM whereas 13 were upregulated and 11 were downregulated in FLDM (Figure 2B).

Using scatterplots for mean Log2FC of total poly(A) in BMDM vs. FLDM, we compared responses of the two macrophage populations to hypoxia for transcripts associated with cell metabolism side-by-side (Figure 2C). While BMDM showed statistically increased levels of transcripts for glycolysis-associated enzymes, FLDM showed similar, albeit not statistically significant, trends for Pgk1, Tpi1, Aldoa, and Ldha. Downregulation of several mitochondria-encoded transcripts (mt-Nd1, mt-Nd2, mt-Cytb) was remarkably similar in BMDM and FLDM in direction and magnitude. Yet there were several notable differences. BMDM showed a significant reduction in abundance of the transcript for an antioxidant enzyme peroxiredoxin-1 (Prdx1) whereas FLDM induced this transcript. The transcript encoding eukaryotic translation elongation factor 1 alpha 1 (Eef1a1) displayed the opposite pattern of changes in response to hypoxia. Only FLDM showed upregulation of ferritin light chain 1 (Ftl1) and down-regulation of mt-Co1 and transcripts encoding ribosomal proteins Rpl32 and Rpl18a. In contrast, only BMDM strongly upregulated the transcript for glucose-6-phosphate isomerase 1 (Gpi1). Thus, besides the shared changes in mitochondria-encoded

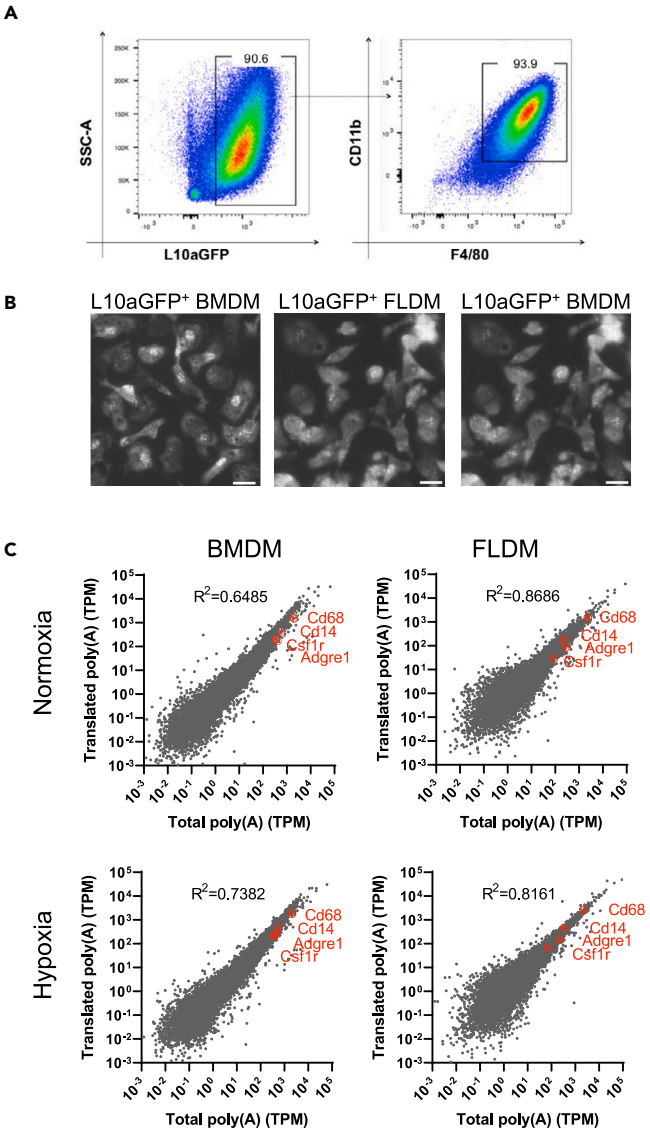

Figure 1. Characterization of BMDM and FLDM phenotype, expression of EGFP-L10 and total vs. translated poly

(A) RNA pools at baseline (normoxia) and after exposure to hypoxia. (A) Representative FACS plots reveal that more than 90% of L10aGFP+ cells in FLDM cultures are F4/80+CD11b+ by day 6 of culture in the presence of M-CSF. Similar pattern of staining was routinely observed in BMDM cultures.

(B) Representative fluorescence microscopy images display EGFP-L10a expression in the differentiated BMDMs and FLDMs from Csf1r^{iCre}L10aGFP+ mice compared to L10aGFP^{-} control. Scale bar = 20 μm.

(C) Normalized results of RNA-seq (TPM) of total vs. translated poly(A) pools for both macrophage types under normoxic and hypoxia conditions. The data are mean of 3 (BMDM) or 2 (FLDM) independently processed samples. Red encircled dots indicate the abundance and translation of mRNA encoding macrophage markers Adgre1 (F4/80), Csf1r (c-fms, or colony stimulating factor 1 receptor), CD14 and CD68. See also Figure S1.

transcripts and a subset of glycolysis associated transcripts, BMDM and FLDM show distinct patterns of responses to hypoxia in transcripts related to protein synthesis and other metabolic pathways.

Among the transcripts associated with immune regulation, platelet factor 4 (Pf4) was significantly upregulated by hypoxia in BMDM and FLDM (Figure 2D). The transcript for complement receptor C5ar1 was significantly upregulated in BMDM with a similar trend in FLDM. Only BMDM displayed an increase in macrophage migration inhibitory factor (Mif) and vimentin (Vim) transcripts, and a decrease in the Ly6e transcript. While FLDM induced chemokine transcripts Ccl7, Ccl2, and Ccl4, BMDM showed significant downregulation of Ccl7 and a trend toward reduction of Ccl2 and Ccl4 mRNA levels, suggesting differential expression of the Ccl chemokines by BMDM and FLDM in response to hypoxia.

Canonical pathway analyses of hypoxia-induced changes in total mRNA expression revealed shared pathways that were significantly affected in BMDM and FLDM (Figure 2E; Table S1). Oxidative phosphorylation showed marked inactivation in both types of macrophages

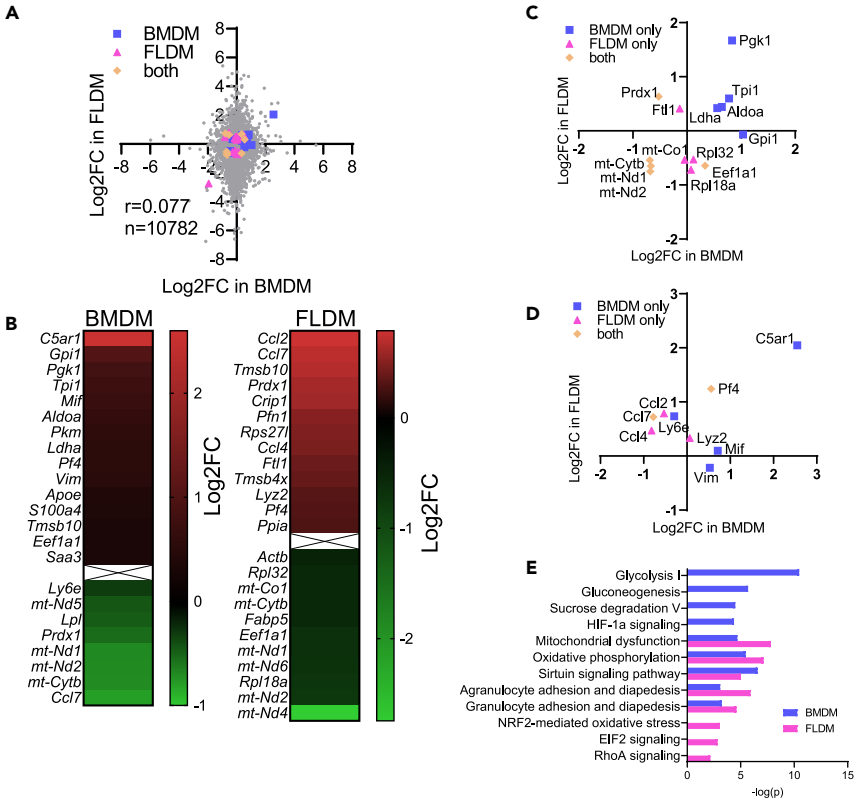

Figure 2. Analyses of changes in the total mRNA abundance in BMDM and FLDM in response to hypoxia

(A) Scatterplot showing Log2FC of total poly(A) in response to hypoxia. Protein-coding transcripts showing statistically significant change in BMDM, FLDM, or both macrophage populations are marked with colors. Spearman's rank correlation (r) and the number of compared transcripts (n) are shown.

(B–D) (B) Heatmap of the protein-coding transcripts that significantly increased or decreased in abundance in each macrophage subset. Log2FC scatterplots of total poly(A) RNA in BMDM vs. FLDM are shown for selected transcripts associated with cell metabolism (C) or immune (D) regulation. The data are mean Log2FC of total poly(A) RNA.

(E) Canonical pathways identified by analyses of the hypoxia-induced changes in total mRNA in BMDM and FLDM. The data are mean of 3 (BMDM) or 2 (FLDM) independently processed samples. See also Figure S2.

(*Z* score = −2 in BMDM and −2.236 in FLDM). Mitochondrial dysfunction and sirtuin signaling were similarly apparent in both types of macrophages, mainly due to downregulation of mitochondria-encoded mRNAs, although z-scores for these pathways did not show significant directional change. Hypoxia-induced changes in C5a1 and chemokine mRNA expression were linked to disturbance of granulocyte and agranulocyte adhesion and diapedesis pathways in both macrophage types, albeit this was due to different transcript subsets and did not show significant directional change. BMDM significantly activated glycolysis I (*Z* score = 2.236) and HIF-1α signaling (*Z* score = 2) pathways. Gluconeogenesis and sucrose degradation pathways were disturbed in BMDM only, while NRF2-mediated oxidative stress, EIF2 signaling and RhoA signaling pathways were disturbed in FLDM only, although without directional change.

We also carried out 3 independent validation experiments with BMDM and FLDM and measured changes in the abundance of selected target mRNA by qRT-PCR (Figure S2). We observed an increase in the abundance of Pgk1 and Tpi1 and a decrease in the abundance of mt-Nd2 RNA both in BMDM and FLDM, in agreement with the RNA-seq analyses of the total poly(A) RNA. Vim mRNA was consistently induced in both macrophage populations, whereas Pf4 mRNA expression showed a trend toward increase, more consistent in FLDM.

Collectively, changes among the total poly(A) transcripts indicate that hypoxia responses in BMDM and FLDM can be characterized by a common pattern in downregulation of mitochondria-encoded transcripts and, to some degree, induction of several glycolysis-associated transcripts. However, BMDM and FLDM show differential changes in the abundance of a subset of transcripts associated with protein synthesis, antioxidant responses, and innate immunity.

Hypoxia-induced changes in translated poly(A) RNA

RNA-seq analyses of the translated poly(A) RNA showed weak correlation of hypoxia-induced changes between BMDM and FLDM (Figure 3A). Among the protein-coding transcripts, 23 were significantly upregulated and 6 were significantly downregulated in BMDM whereas only 3 were upregulated and 6 were downregulated in FLDM (Figure 3B).

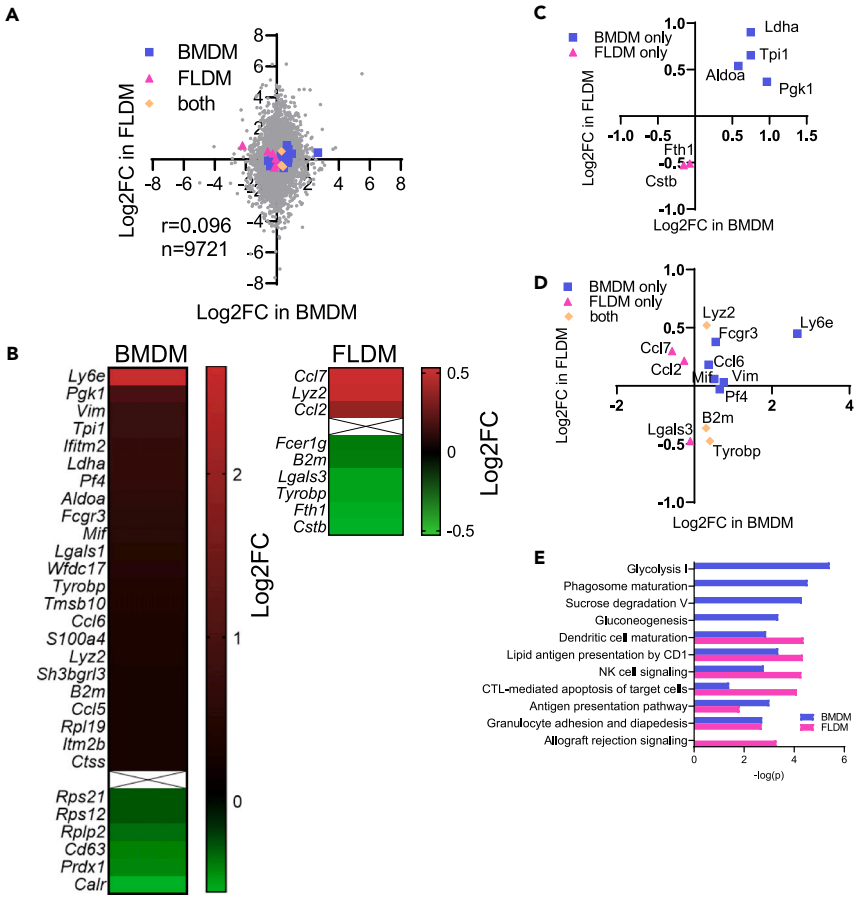

Figure 3. Analyses of the changes in translated mRNA in BMDM and FLDM in response to hypoxia

(A) Scatterplot showing Log2FC of translated poly(A) in response to hypoxia. Protein-coding transcripts showing significant change in BMDM, FLDM, or both macrophage populations are marked with colors. Spearman's rank correlation (r) and the number of compared transcripts (n) are shown.

(B–D) (B) Heatmap of the mRNAs that displayed significantly increased or decreased translation in each macrophage subset. Log2FC scatterplots of translated poly(A) RNA in BMDM vs. FLDM are shown for selected transcripts associated with cell metabolism (C) or immune (D) regulation. The data are mean Log2FC for translated poly(A) RNA.

(E) Canonical pathways identified by analyses of the hypoxia-induced changes in translated mRNAs in BMDM and FLDM. The data are mean of 3 (BMDM) or 2 (FLDM) independently processed samples.

We plotted the Log2FC of translated poly(A) in BMDM vs. FLDM to compare translational responses of the two macrophage populations to hypoxia. Although the increased translation of enzymes involved in glycolysis (Pgk1, Tpi1, Ldha, and Aldoa) was statistically significant only in BMDM, similar trends were observed in FLDM (Figure 3C). In contrast, downregulation of translation of ferritin heavy chain 1 (Fth1) and cystatin B (Cstb) was evident only in FLDM. Translation of immune-associated transcripts (Ly6e, Fcgr3, Ccl6) was significantly increased in BMDM with similar trends observed in FLDM whereas translation of Lyz2 significantly increased in both macrophage populations (Figure 3D). While significantly increased translation of Mif, Vim, Pf4 was observed in BMDM, there were no changes in translation of those transcripts in FLDM. Finally, increased translation of B2m and Tyrobp and decreased translation of Ccl7 and Ccl2 in BMDM was accompanied by the opposite changes or trends in FLDM.

Canonical pathway analyses of hypoxia-induced translational changes linked responses to hypoxia with pathways for glycolysis I, phagosome maturation, sucrose degradation and gluconeogenesis in BMDM and allograft rejection signaling in FLDM (Figure 3E; Table S2). Several pathways (dendritic cell maturation, lipid antigen presentation by CD1, NK-signaling, CTL-mediated apoptosis of target cells, antigen presentation, and granulocyte adhesion and diapedesis) were shared by BMDM and FLDM, although they were represented by few transcripts that were either regulated in different directions (translation of Tyrobp and B2m increased in BMDM and decreased in FLDM) or were distinct (Fcgr3, Calr, Ccl5, Ccl6, PF4 in BMDM vs. Fcerg1, Ccl2, Ccl7 in FLDM).

Next, we determined the relationships between changes in translated vs. total poly(A) RNA by plotting hypoxia-induced Log2FC of total vs. translated poly(A) RNA (Figures 4A and 4B). In BMDM, the Log2FC of translation of most transcripts correlated with the Log2FC of their abundance. However, Ly6e and C5ar1 transcripts showed opposite relationships in their abundance and translation. In FLDM, the overall

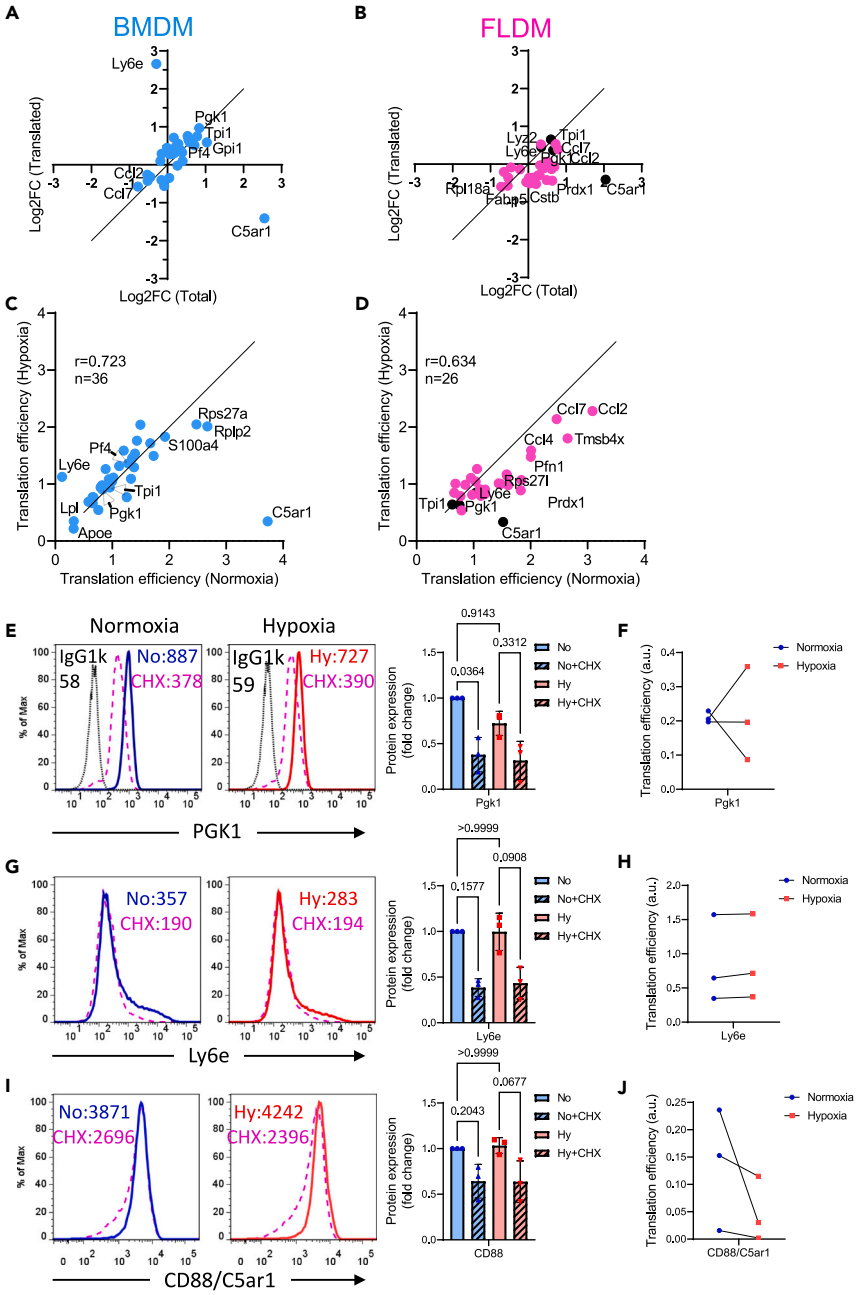

Figure 4. Scatterplots of Log2FC of total vs. poly(A) transcripts in BMDM (A) and FLDM (B) after hypoxia

Only transcripts that showed significant change in abundance or translation in BMDM are shown in (A). In addition to the transcripts that showed significant change in abundance or translation in FLDM, Log2FC values for Ly6e, Tpi1, Pgk1 and C5ar1 in FLDM are shown in black for comparison with BMDM. Mitochondria encoded transcripts were excluded from both panels. The straight lines show linear regression for equal change in Log2FC representing a model of equal change in mRNA abundance and translation. Translation efficiency for hypoxia-regulated transcripts in BMDM (C) and FLDM (D). Spearman's rank correlation (r) and the number of compared transcripts (n) are shown. Protein expression levels measured by flow cytometry and estimation of the translation efficiency (calculated as the ratio of the change in protein abundance after CHX treatment to the corresponding mRNA abundance) for PGK-1 (E,F), Ly6e (G, H), and CD88/C5ar1 (I, J). Representative FACS plots, mean ± SD and individual fold change in protein expression and translation efficiency values of three independent experiments are shown. Nonparametric Kruskal-Wallis analyses of variance followed by Dunn's multiple comparisons of the experimental groups were carried out for data in E, G, and I (*, $p < 0.05$, $n = 3$). See also Figure S3.

Log2FC of translation also correlated with the Log2FC of mRNA abundance. However, some transcripts (Prdx1, Cstb, C5ar1) displayed a trend toward reduced translation despite increased abundance.

Calculating the ratio of specific transcripts in translated to total poly(A) fractions isolated from the same samples of homogeneous cells in culture enabled effective measurement of changes in translation efficiency for those transcripts in response to hypoxia. Translation efficiency for transcripts that were regulated by hypoxia BMDM and FLDM showed relatively strong correlation between normoxic and hypoxic conditions (Figures 4C and 4D). In BMDM, hypoxia decreased the translation efficiency of C5ar1 and increased the translation efficiency of Ly6e. In FLDM, exposure to hypoxia reduced the translation efficiency for several transcripts (Ccl2, Ccl7, Ccl4, Pfn1, Prdx1, Rps27l, and C5ar1).

To assess the impact of prolyl hydroxylase domain enzymes (PHDs) on changes in total and translated transcripts, as well as translation efficiency, we treated BMDM with 0.1 mM dimethyloxaloylglycine (DMOG), a well characterized pan-PHD inhibitor. As expected, DMOG induced the transcripts for glycolysis-associated enzymes (Pgk1, Tpi1, Ldha, and Gapdh), but did not impact the levels of mitochondrial mt-Nd2 mRNA (Figure S3A). Using the L10a-EGFP TRAP assay followed by qRT-PCR, we also measured the Log2FC of total and translated transcripts after treatment with DMOG or exposure to hypoxia. Although treatment with DMOG was more efficient than hypoxia to increase total and translated Pgk1, Tpi1, Ly6e and PF4 (Figure S3B), both treatments had essentially identical effects on translation efficiency (Figure S3B). Translation efficiency of Tpi1 and PF4 transcripts was relatively low at baseline and changed little after hypoxia or DMOG treatment. On the other hand, translation efficiency of Ly6e and C5ar1 was higher at baseline and showed similar upward trends after hypoxia or DMOG treatment. Interestingly, while translation efficiency of Pgk1 appeared remarkably high at the baseline, it showed a downward trend after hypoxia and DMOG treatment. Overall, these results suggest that inhibition of PHDs has similar effects on induction and translation of transcripts in question.

To determine whether the assessments of translation rate and efficiency obtained by TRAP analyses correlate with protein synthesis, we measured expression levels of PGK-1, Ly6e, and CD88 (encoded by C5ar1) by FACS in BMDM under normoxia and hypoxia conditions. Addition of the protein synthesis inhibitor cycloheximide (CHX) enabled us to determine the fraction of the newly synthesized proteins (i.e., translation rate) and, in combination with the specific mRNA quantification, to estimate the translation efficiency (Figures 4E–4J). Hypoxia exposure did not appear to result in significant changes in expression of the proteins in question. However, treatment with CHX resulted in statistically significant decreased levels of PGK-1, thus supporting the important role of protein synthesis in maintenance of its expression under normoxic and hypoxic conditions. Due to concerns that FACS analyses of PGK-1 protein may miss some of the specific signal, we performed immunoblotting (Figure S3D). Hypoxia led to a small increase in the dominant ~45 kDa band corresponding to the predicted molecular weight of full-length PGK-1. Smaller molecular weight minor bands, likely representing PGK-1 degradation products, were also increased in intensity. The combined densitometry signal showed a small (5–20%) increase when normalized to actin. Calculated translation efficiency (change in the protein level after CHX treatment normalized to Pgk1 mRNA from parallel samples) was lower after exposure to hypoxia. In aggregate, these data suggest that despite a significant induction of Pgk1 mRNA, PGK-1 protein levels only minimally rose in macrophages after exposure to hypoxia. Ly6e and CD88/C5ar1 showed a trend toward decreased levels after CHX treatment, albeit not reaching statistical significance. The estimated translation efficiency was variable from experiment to experiment and overall showed no change for PGK-1 and Ly6e with a trend toward decrease of CD88/C5ar1 (Figures 4F, 4H, and 4J). FACS/qRT-PCR-based estimates of translation efficiency for Pgk1 and C5ar1 were consistent with the TRAP-based estimates (Figures 4C, 4F, and 4J), but showed discordance for Ly6e. It is likely that heterogeneity of Ly6e expression in BMDM interfered with accurate assessment of protein translation.

Effects of HuR deletion on hypoxia-induced changes in mRNA abundance and translation in BMDM and FLDM

To determine whether HuR regulates responses to hypoxia in BMDM and FLDM, we analyzed hypoxia mRNA profiles in BMDM and FLDM isolated from Csf1r^{iCre}Rosa26$^{EGFP-L10a}$ mice crossed to Hur$^{fl/fl}$ mice[23] (Figure 5). Efficiency of HuR deletion in cultured macrophages exceeded 94% while hypoxia had minimal effects on HuR expression in WT cells (Figure S4). Deletion of HuR had a profound impact on the hypoxia-induced changes in mRNA abundance and translation. Of the 23 transcripts that were upregulated or downregulated by hypoxia in wild-type BMDM, only 8 transcripts showed a significant change in the same direction (Tpi1, Pkm, Ldha, Saa3, Lpl, mt-Nd1, mt-Nd2, and mt-Cytb) in HuR-KO BMDM. While hypoxia resulted in significant changes in translation of 27 transcripts in wild-type BMDM, translation of only 5 transcripts (Mif, Lgals1, Tmsb10, Prdx1, and Rps12) changed in the same direction in HuR-deleted BMDM. Of the 24 transcripts that were either upregulated or downregulated by hypoxia in wild-type FLDM, only 5 transcripts (Ftl1, Lyz2, mt-Cyb, mt-Nd2, and mt-Nd6) were significantly similarly affected in the HuR-KO FLDM. Remarkably, of the 9 transcripts that were differentially translated in response to hypoxia in FLDM, only Fth1 showed a statistically significant decrease in translation in HuR-deleted FLDM. These results suggest that hypoxia-induced changes in mRNA abundance and translation are dependent to a large extent on HuR.

Next, we analyzed the direction of the HuR-deletion on responses to hypoxia by focusing on transcripts that showed increased translation in wild-type macrophages. In BMDM, hypoxia-driven increases in both abundance and translation of Pgk1, Tpi1, Pf4, and Vim were blunted by HuR deletion (Figure 5B). On the other hand, deletion of HuR resulted in a slightly higher increase in Mif mRNA translation despite a less profound increase in its abundance. Furthermore, HuR deletion slightly blunted increases in translation of Fcgr3, Ldha, and Ifitm2, but had an opposite effect on hypoxia-induced changes in Fcgr3 and Ldha mRNA abundance. Most striking was the effect of HuR deletion on hypoxia-induced changes in Ly6e expression: although wild-type BMDM responded to hypoxia by increasing Ly6e translation with a trend toward decreased abundance, HuR-deleted macrophages responded to hypoxia by reduction of Ly6e translation and a dramatic increase in abundance (Figure 5C). In FLDM, HuR deletion blunted hypoxia-induced increases in Ccl7 and Ccl2 translation and abundance, but blunted translation of Lyz2 mRNA with minimal impact on its abundance (Figure 5D).

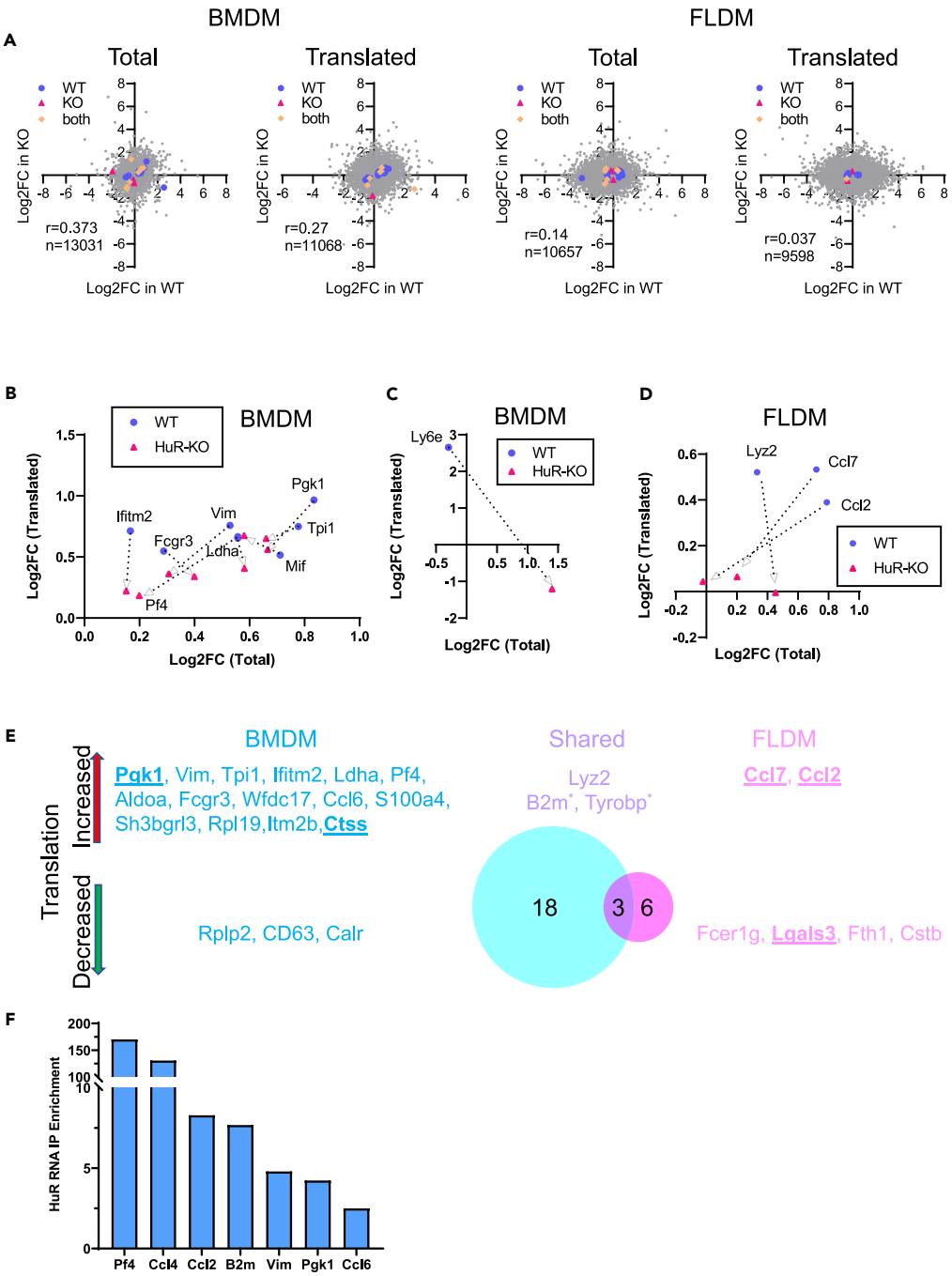

Figure 5. Effects of HuR deletion in macrophages on abundance and translation of mRNA transcripts regulated by response to hypoxia

(A) Scatterplot showing Log2FC of total and translated poly(A) in response to hypoxia. Protein-coding transcripts showing significant change in wild-type, HuR-KO, or both are marked with colors. Spearman's rank correlation (r) and the number of compared transcripts (n) are shown.

(B) and (C). Effects of HuR deletion on select transcripts that showed significant increase in translation in BMDM.

(D) Effects of HuR deletion on transcripts that showed significant increase in translation in FLDM.

(E) BMDM- or FLDM-specific or shared mRNAs showing hypoxia-induced change in translation in HuR-dependent mode. Previously described HuR targets are underlined in bold font. Asterisk (*) indicates increased translation in BMDM but decreased translation in FLDM.

(F) Enrichment of the transcripts in the HuR-RNA IP pulldown. The data are mean of 3 independently processed samples. The data in panel F are representative of two independent experiments. See also Figure S4.

In aggregate, RNA-seq translational profiling of wild-type and HuR-deleted BMDM and FLDM identified distinct mRNAs that are regulated by HuR in response to hypoxia (Figure 5E). Within the shared subset, translation of Lyz2 increased in both cell populations, whereas translation of B2m and Tyrobp increased in BMDM, but decreased in FLDM. The BMDM-specific, HuR-regulated subset of transcripts encode enzymes involved in glycolysis, ribosomal proteins and regulators of immune responses. All FLDM-specific HuR-regulated transcripts identified in this study encode proteins with described immune functions, five of which previously have been shown to be targets of HuR regulation in other cell types: Pgk1, Ctss, Ccl2, Ccl7, and Lgals3.[41–44] Other transcripts may represent novel targets of regulation by HuR.

To determine whether HuR may exert direct effects on the indicated transcripts, we measured HuR binding to the candidate transcripts by carrying out RNA-immunoprecipitation (IP) followed by qRT-PCR assays (Figure 5F). Enrichment of the Pf4 and Ccl4 transcripts in the HuR RNA-IP pulldown exceeded enrichment of Vegfa mRNA, another well described target of HuR in macrophages.[23,45] Several transcripts (Ccl2, B2m, Vim, Pgk1, and Ccl6) were also enriched in the HuR-RNA IP pulldowns, albeit at lower levels (Figure 5F). Others (Ccl7, Ly6e, Lgals3, Lyz2, Ifitm2, Tyrobp, and Tpi1) were present in the HuR and isotype control RNA-IP complexes at similar levels (not shown), suggesting a possible role of indirect mechanisms of regulation by HuR.

To demonstrate HuR-dependent, hypoxic regulation of gene expression in macrophages *in vivo*, we used our previously described $HuR^{fl/fl}$ and LysM-cre mouse cross, achieving myeloid cell-specific HuR deletion *in vivo*,[23] and employed the ear punch hole injury model.[46–48] In this model, the ear wound area reduces over time due to tissue repair, at times resulting in complete closure.[46–48] Increased expression and activation of HIF-1α (tissue hypoxia-triggered) has been shown to induce wound repair in C57BL/6 mice.[47] Consistent with prior studies,[46–48] the ear tissue surrounding the wound appeared inflamed and hemorrhaged at day 4 post-injury (Figure 6A). As inflammation receded after day 7, the open wound area decreased with 4 out of 8 WT mice showing complete closure by day 35. The open wound area was significantly higher in the myeloid HuR-KO compared to the WT mice and none of the 6 HuR-KO mice showed complete closure by day 35 (Figure 6B).

To measure changes in mRNA and protein expression in response to the injury, we collected the inflamed ear tissue on day 4 post injury by centering a 6-mm punch on the open wound. Intact contralateral ear tissue samples were collected with another 6-mm ear punch and processed as controls. Ccl2, an HuR target that we observed in our macrophage profiling screen, was induced more than 2-fold in the inflamed tissue in the WT, but not in the HuR-KO mice (Figure 6C). The effect was specific for Ccl2 mRNA, as Hif1a and Cd68 mRNA showed no apparent induction and no difference between the WT and HuR-KO mice. Induction of Ccl2 mRNA in the inflamed tissue resulted in greater abundance of Ccl2 protein in the WT, but not in the HuR-KO, mice (Figure 6D), supporting that macrophage HuR is required for induction of Ccl2 mRNA and protein in response to (hypoxic) injury.

DISCUSSION

We characterized total and translated poly(A) RNA in differentiated macrophages of embryonic (FLDM) and adult (BMDM) origin at baseline and after exposure to hypoxia at the whole transcriptome level. We expected to observe both similarities and distinctions between BMDM and FLDM in translated mRNAs. Indeed, the mRNAs encoding macrophage-specific markers F4/80/Adgre1, Csfr1, CD14, and CD68 were expressed and translated at high levels and did not change in response to hypoxia in BMDM and FLDM. Translation of the myeloid lysozyme M (Lyz2) increased after hypoxia in both macrophage types. BMDM and FLDM responded similarly to hypoxia by decreasing abundance of mitochondria-encoded mRNAs in the total poly(A) RNA. Augmented expression of transcripts encoding glycolytic enzymes, both at the level of total poly(A) RNA and of translation, was statistically significant in BMDM and showed a similar trend in FLDM. Importantly, BMDM and FLDM showed striking differences in the induction of chemokines and several other transcripts encoding immune regulators. While BMDM increased translation of Ly6e, Ifitm2, Pf4, Fcgr3, Mif, Tyrobp, Ccl6, and Ccl5, and decreased translation of Calr, FLDM increased translation of Ccl2 and Ccl7 and decreased translation of Fcer1g, Lgals3, Tyrobp, and Fth1. Overall, these findings support our hypothesis that embryonic and adult macrophages respond to hypoxia by changing translation of distinct mRNA subsets.

Application of the L10a-GFP TRAP assay in combination with RNA-seq of total poly(A) and ribosome-associated poly(A) RNAs enabled assessment of translation rate and efficiency for specific transcripts. Given abundant posttranscriptional regulatory influences on mRNA stability and translation, we expected differences between hypoxia-induced total and actively translated mRNA profiles. Increased or decreased translation in response to hypoxia could be explained by similar changes in mRNA abundance for approximately one-third of transcripts (10/29 in BMDM and 3/9 in FLDM). In FLDM, chemokines Ccl2 and Ccl7 were among the most induced transcripts, while also showing increased translation. However, despite the significant induction of the transcripts for Ccl2, Ccl7, Prdx1, Pfn1, and Rps27l in FLDM, their translation efficiency seemed to decline after hypoxia (Figure 4D). It is possible that ribosome association of highly induced transcripts may lag behind their transcription, similar to what was previously described for LPS-induced transcripts.[33,49]

Some the of the differentially translated transcripts showed opposite trends in their abundance (e.g., Ly6e in BMDM and C5ar1 in BMDM and FLDM). Using an independent assay (combination of flow cytometry with CHX treatment and qRT-PCR), we validated the observation that translation efficiency of C5ar1 is lower under hypoxia conditions (Figure 4J). This may explain why protein levels of CD88 (encoded by C5ar1) did not increase despite a rather dramatic induction of C5ar1 mRNA. Those data suggest that C5ar1 could be a target of specific translation repression under hypoxia and separate mechanisms regulating mRNA abundance and translation may be engaged in response to hypoxia. Further studies will be necessary to determine the exact nature of the upstream regulators and their point of action, such as regulation of transcription or mRNA turnover vs. translational control.

General protein synthesis is reduced under hypoxic conditions due to energy starvation.[9,10] However, translation of a subset of transcripts can not only proceed, but increase through formation of alternative translation initiation complexes dependent on binding of HIF-2α to the hypoxia response elements at the 3′UTR or cap-independent mRNA translation from the internal ribosome entry site (IRES).[14–16] Since

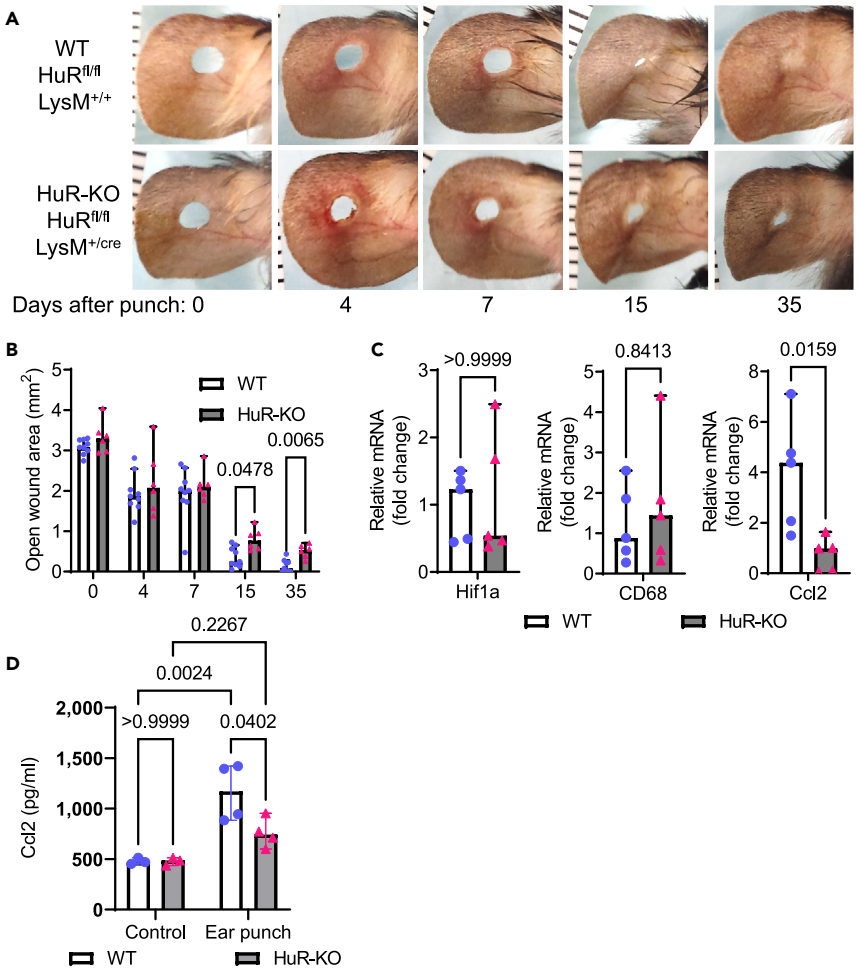

Figure 6. Macrophage HuR dependence of Ccl2 mRNA and protein induction in a mouse model of tissue injury

(A and B) Representative images (A) and measurements of the wound area (B) after 2-mm ear punch. Individual animal data and median ± 95%CI are shown; n = 8 for WT and n = 6 for HuR-KO mice. Ruler scale = 1 mm.

(C) Abundance of Hif1a, CD68, and Ccl2 mRNA in the control ear tissue and the ear tissue in the area surrounding the ear punch hole ("donut" obtained by centering the 6-mm punch on the open wound) was measured by qRT-PCR on day 4 post injury. The data were expressed as fold change in the inured vs. control samples (individual animal samples and median ± 95%CI are shown); n = 5.

(D) Ccl2 (MCP-1) protein was measured by ELISA in the control and injured tissue samples collected as described above on day 4. Individual animal data and median ± 95%CI are shown; n = 3 for control and n = 4 for ear punch samples. Statistical analyses are marked by brackets with p values: two-way ANOVA followed by Šídák's multiple comparisons between WT and HuR-KO in (B), Mann-Whitney non-parametric test in (C) and two-way ANOVA followed by Tukey's multiple comparisons test.

cap-independent translation requires L10a,[50] the use of the EGFP-L10a TRAP for translational profiling may have enabled identification of transcripts undergoing cap-independent translation. Several transcripts predicted to have an IRES in their 5′UTR showed increased (Ly6e, Tpi1, Ifitm2, Ldha, Mif, S100a, Ctss) or decreased (CD63, Calr) translation in BMDM or decreased (Cstb) translation in FLDM.

We examined how the RNA-binding protein HuR regulates mRNA abundance and translation in macrophage responses to hypoxia (Figure 5). Using the same Csf1r-iCre driver as for the L10a-EGFP expression, we deleted HuR in differentiated macrophages and carried out the L10a-GFP TRAP assays followed by RNA-seq. By comparing the hypoxia-induced changes in total and translated poly(A) in wild-type vs. HuR-deleted macrophages, we identified transcripts that required HuR for differential translation (Figure 5). While several transcripts, such as Pgk1, Ctss, Ccl2, Ccl7, and Lgals3, were previously described as direct targets of HuR in cell types other than macrophages,[41–44] this study is the first to describe how they are regulated by HuR in embryonic vs. adult-derived macrophages in response to hypoxia. Moreover, we identified 22 additional potential targets of HuR-dependent post-transcriptional regulation. Of those, 7 transcripts (Pf4, Ccl4, Ccl2, B2m, Vim, Pgk1, Ccl6) appear to be direct targets of HuR as demonstrated by HuR binding assays (Figure 5F). Other transcripts may apparently be regulated by HuR indirectly. The exact mechanism of the HuR-dependent regulation will be the subject of future studies.

Detection of mitochondria-encoded transcripts in total poly(A) fractions (Figure 2) was not surprising, given that mammalian mitochondrial mRNAs are post-transcriptionally polyadenylated with approximately 55 A residues by mitochondrial poly(A) polymerase.[51] Hypoxia-induced downregulation of multiple mitochondria-encoded transcripts within the total poly(A) RNA pool in BMDM and FLDM most likely represents mitochondrial dysfunction, as a universal response of the mitochondrial transcriptome to hypoxic conditions.[52]

The L10a protein used for affinity purification of the translated poly(A) RNA is a constitutive component of the 60S subunit, one of the subunits of the 80S ribosome.[35] Since mitochondrial mRNAs are translated by the mitochondrial 55S ribosome without involvement of the 80S ribosome,[51] the translated poly(A) RNA pools should be depleted of mitochondrial transcripts. In fact, mitochondrial transcripts in the translated poly(A) pools were reduced by ~50-fold when compared to the total poly(A) pools (Figure S1). It is likely that high abundance of mitochondria mRNA in macrophages may have resulted in a small contamination of the TRAP reactions.

While mitochondrial dysfunction in response to hypoxia was shared by BMDM and FLDM, hypoxia-induced activation of glycolysis pathways, as evidenced by increased abundance and translation of several mRNAs encoding glycolytic enzymes, was clearly preferential for BMDM and indicates metabolic reprogramming. It remains to be determined whether translation of glycolysis-related mRNAs in FLDM at baseline is sufficient to provide for increased glycolytic demands under hypoxic conditions. It is possible that activation of the HIF-1α pathway by hypoxia in BMDM leads to transcriptional activation of *Pgk1, Tpi1, Aldoa, and Ldha* genes, with increased abundance of the corresponding mRNAs leading to increase in their translation. We cannot rule out a possibility that the apparent dependence of increased Pgk1, Tpi1, Aldoa, and Ldha on HuR expression is due, at least in part, to indirect effects of HuR on gene transcription, such as previously described stabilization of Hif1a mRNA by HuR.

Hypoxia-induced changes in BMDM and FLDM mRNA translation included a number of mRNAs encoding immune regulators, although the repertoire of those mRNAs was different between the macrophage types. Increased translation of RNAs encoding CC-chemokines Ccl7 and Ccl2 in FLDM is consistent with the previously described induction of alveolar macrophage Ccl2 in response to hypoxia *in vivo*,[53] since alveolar macrophages are largely FLDM-derived.[54,55] Using a well-characterized ear punch model and conditional deletion of HuR in macrophages, we demonstrated that macrophage HuR is necessary for induction of Ccl2 mRNA and protein after injury (Figure 6). We used the LysM-cre driver to delete HuR since it is more myeloid cell-specific than the Csf1r-iCre driver (reported to also be active in lymphoid cells).[34] Ccl2 is necessary for proper wound healing[56,57] and tissue repair after myocardial infarction.[58] Dermal resident macrophages of apparently embryonic origin are abundant in the mouse ear[59,60] and known to contribute to regulation of tissue homeostasis.[61] Our findings in this model are consistent with our macrophage screening results, supporting that HuR mediates repair functions of resident macrophages through regulation of gene expression in relatively hypoxic wounded tissues. Thus, it appears that macrophages of embryonic origin respond to hypoxia by recruiting more myeloid cells via production of Ccl2 and Ccl7. This amplified inflammation could result in augmented injury but, in many settings, such as wound closure, is important in the reparative process. On the other hand, BMDM showed increased translation of a functionally different subset of chemokines (Pf4, Ccl6, and Ccl5). Our results suggest that the origin of macrophages determines the repertoire of newly synthesized chemokines in response to hypoxia. These phenotypic and functional differences could be significant in the context of myocardial ischemia or other organ responses to hypoxic injury *in vivo*. Most importantly, there may be opportunities to therapeutically exploit these differences, thereby favoring production of protective factors from the myeloid population most highly localized to a given pathologic site.

Limitations of the study

The main limitation of the study was the need to isolate precursors and differentiate BMDM and FLDM *in vitro* from different (albeit genetically identical) animals. To mitigate the risk, we carefully maintained identical cell culture conditions, using the same lots of the cell culture media and supplements. *In vitro* differentiation under the same conditions, although necessary, may have reduced the differences in total and translated transcripts between the two macrophage populations. Another limitation was the need to isolate the samples from BMDM and FLDM on different days. To avoid the potential risks of misinterpretation due to timing, we analyzed the responses to hypoxia as fold change (or Log2FC) for translated and total RNA within each sample and within the group, avoiding direct comparison of the RNA-seq data (TPM) between BMDM and FLDM without normalization to internal controls.

The L10a-EGFP-based TRAP assay has been used to assess translation in multiple systems and enabled us to measure total and translated poly(A) RNA in a single workflow, estimating transcriptome-wide translation efficiency. However, the inherent limitation of this approach is that it measures only ribosome occupancy, one of several possible determinants of translation rate and efficiency. We used CHX inhibition to block protein synthesis and measured specific protein amount with or without CHX by flow cytometry (PGK-1, Ly6e, CD88/C5ar1) and immunoblotting (PGK-1) and the corresponding mRNA abundance by qRT-PCR to estimate translation efficiency. Considerable baseline protein levels for PGK-1, Ly6e, and CD88 with lack of protein level changes after exposure to hypoxia confounded our efforts to provide definitive proof that hypoxia changed the mRNA translation efficiency for those targets. Furthermore, we relied on assumption that hypoxia did not alter the protein half-life for PGK-1, Ly6e, and CD88 but acknowledge that the analyses would be more complex for proteins with half-lives affected by hypoxia. Additional studies involving alternative approaches for *direct* measurement of global and target-specific translation are necessary to establish how hypoxia regulates translation efficiency of PGK-1, Ly6e, CD88 and of other targets identified in this report. That is, direct assays for protein translation using pSILAC or O-propargyl-puromycin labeling of nascent polypeptides coupled with RNA-seq analyses of total RNA may provide better assessment of translation efficiency.

STAR★METHODS

Detailed methods are provided in the online version of this paper and include the following:

SUPPLEMENTAL INFORMATION

Supplemental information can be found online at https://doi.org/10.1016/j.isci.2023.107985.

ACKNOWLEDGMENTS

Special thanks to Drs. Chris Castaldi and Sameet Mehta at Yale Center for Genome Analyses who performed RNA-seq and provided bioinformatics support, respectively, and to Dr. Fatima Zahra Saddouk for assistance with the hypoxia protocol. We thank Dr. Bryan Young (Yale University School of Medicine) for his advice and efforts in crossing the L10a-EGFP mice with Csf1r-iCre mice and Rachel Rivera (Yale University) for her assistance with qRT-PCR assays. We also thank faculty and staff at HHMI and in the Yale School of Medicine Office of Student Research (OSR), who provided essential administrative support. We acknowledge our funding sources, including the Howard Hughes Medical Institute (HHMI) Medical Research Fellowship (2017–2018, NSW), the Yale School of Medicine Marvin Moser Research Fellowship (2018, NSW), NIH/DHHS R01GM126412 (JRB) and the Connecticut Biomedical Research Fund (JRB).

AUTHOR CONTRIBUTIONS

N.S.W. and T.O.Y. designed and performed TRAP experiments, analyzed and visualized the data, prepared the figures, and co-wrote the paper. P.P. performed BMDM and FLDM isolation and differentiation, isolated RNA and performed qRT-PCR and immunoblotting assays. V.S.R. assisted with the design of the animal genotyping assays, verified the data analyses, contributed to data visualization and edited the manuscript. A.M. performed the initial RNA-seq and gene ontology analyses. Y.W. provided guidance and assistance with timed animal breeding, embryo and FLDM isolation, S.N. provided expert intellectual input and guidance for RNA-seq data analyses and edited the manuscript. K.K.H. provided expert guidance for the FLDM isolation and study design. J.R.B. conceptualized the project, secured funding, designed, and supervised the experimental work and data analyses, co-wrote and edited the manuscript.

DECLARATION OF INTERESTS

T.O.Y. reported consulting fees from CaroGen Corporation outside the submitted work. Other authors have no conflict of interests in relation to the subject of this study.

Received: April 20, 2021
Revised: July 21, 2023
Accepted: September 15, 2023
Published: September 21, 2023

REFERENCES

1. Ginhoux, F., and Jung, S. (2014). Monocytes and macrophages: Developmental pathways and tissue homeostasis. Nat. Rev. Immunol. *14*, 392–404. https://doi.org/10.1038/nri3671.
2. Lavine, K.J., Epelman, S., Uchida, K., Weber, K.J., Nichols, C.G., Schilling, J.D., Ornitz, D.M., Randolph, G.J., and Mann, D.L. (2014). Distinct macrophage lineages contribute to disparate patterns of cardiac recovery and remodeling in the neonatal and adult heart. Proc. Natl. Acad. Sci. USA *111*, 16029–16034. https://doi.org/10.1073/pnas.1406508111.
3. Heidt, T., Courties, G., Dutta, P., Sager, H.B., Sebas, M., Iwamoto, Y., Sun, Y., Da Silva, N., Panizzi, P., van der Laan, A.M., et al. (2014). Differential contribution of monocytes to heart macrophages in steady-state and after myocardial infarction. Circ. Res. *115*, 284–295. https://doi.org/10.1161/CIRCRESAHA.115.303567.
4. Epelman, S., Lavine, K.J., Beaudin, A.E., Sojka, D.K., Carrero, J.A., Calderon, B., Brija, T., Gautier, E.L., Ivanov, S., Satpathy, A.T., et al. (2014). Embryonic and adult-derived resident cardiac macrophages are maintained through distinct mechanisms at steady state and during inflammation. Immunity *40*,

91–104. https://doi.org/10.1016/j.immuni.2013.11.019.
5. Dick, S.A., Macklin, J.A., Nejat, S., Momen, A., Clemente-Casares, X., Althagafi, M.G., Chen, J., Kantores, C., Hosseinzadeh, S., Aronoff, L., et al. (2019). Self-renewing resident cardiac macrophages limit adverse remodeling following myocardial infarction. Nat. Immunol. *20*, 29–39. https://doi.org/10.1038/s41590-018-0272-2.
6. Liao, X., Shen, Y., Zhang, R., Sugi, K., Vasudevan, N.T., Alaiti, M.A., Sweet, D.R., Zhou, L., Qing, Y., Gerson, S.L., et al. (2018). Distinct roles of resident and nonresident macrophages in nonischemic cardiomyopathy. Proc. Natl. Acad. Sci. USA *115*, E4661–E4669. https://doi.org/10.1073/pnas.1720065115.
7. Wheaton, W.W., and Chandel, N.S. (2011). Hypoxia. 2. Hypoxia regulates cellular metabolism. Am. J. Physiol. Cell Physiol. *300*, C385–C393. https://doi.org/10.1152/AJPCELL.00485.2010.
8. Fuhrmann, D.C., and Brüne, B. (2017). Mitochondrial composition and function under the control of hypoxia. Redox Biol. *12*, 208–215. https://doi.org/10.1016/J.REDOX.2017.02.012.
9. Liu, L., Cash, T.P., Jones, R.G., Keith, B., Thompson, C.B., and Simon, M.C. (2006). Hypoxia-induced energy stress regulates mRNA translation and cell growth. Mol. Cell *21*, 521–531. https://doi.org/10.1016/J.MOLCEL.2006.01.010.
10. Koumenis, C., Naczki, C., Koritzinsky, M., Rastani, S., Diehl, A., Sonenberg, N., Koromilas, A., and Wouters, B.G. (2002). Regulation of protein synthesis by hypoxia via activation of the endoplasmic reticulum kinase PERK and phosphorylation of the translation initiation factor eIF2alpha. Mol. Cell Biol. *22*, 7405–7416. https://doi.org/10.1128/MCB.22.21.7405-7416.2002.
11. Bishop, T., and Ratcliffe, P.J. (2015). HIF hydroxylase pathways in cardiovascular physiology and medicine. Circ. Res. *117*, 65–79. https://doi.org/10.1161/CIRCRESAHA.117.305109.
12. Semenza, G.L. (2007). Oxygen-dependent regulation of mitochondrial respiration by hypoxia-inducible factor 1. Biochem. J. *405*, 1–9. https://doi.org/10.1042/BJ20070389.
13. Kaelin, W.G., and Ratcliffe, P.J. (2008). Oxygen sensing by metazoans: the central role of the HIF hydroxylase pathway. Mol. Cell *30*, 393–402. https://doi.org/10.1016/J.MOLCEL.2008.04.009.
14. Uniacke, J., Holterman, C.E., Lachance, G., Franovic, A., Jacob, M.D., Fabian, M.R., Payette, J., Holcik, M., Pause, A., and Lee, S. (2012). An oxygen-regulated switch in the protein synthesis machinery. Nature *486*, 126–129. https://doi.org/10.1038/NATURE11055.
15. Chee, N.T., Lohse, I., and Brothers, S.P. (2019). mRNA-to-protein translation in hypoxia. Mol. Cancer *18*, 49. https://doi.org/10.1186/S12943-019-0968-4.
16. Braunstein, S., Karpisheva, K., Pola, C., Goldberg, J., Hochman, T., Yee, H., Cangiarella, J., Arju, R., Formenti, S.C., and Schneider, R.J. (2007). A hypoxia-controlled cap-dependent to cap-independent translation switch in breast cancer. Mol. Cell *28*, 501–512. https://doi.org/10.1016/J.MOLCEL.2007.10.019.
17. O'Neill IV, T.J., Wamhoff, B.R., Owens, G.K., and Skalak, T.C. (2005). Mobilization of bone marrow-derived cells enhances the angiogenic response to hypoxia without transdifferentiation into endothelial cells. Circ. Res. *97*, 1027–1035. https://doi.org/10.1161/01.RES.0000189259.69645.25.
18. Lewis, J.S., Lee, J.A., Underwood, J.C., Harris, A.L., and Lewis, C.E. (1999). Macrophage responses to hypoxia: Relevance to disease mechanisms. J. Leukoc. Biol. *66*, 889–900. https://doi.org/10.1002/jlb.66.6.889.
19. Rahat, M.A., Bitterman, H., and Lahat, N. (2011). Molecular mechanisms regulating macrophage response to hypoxia. Front. Immunol. *2*, 45. https://doi.org/10.3389/FIMMU.2011.00045.
20. McGettrick, A.F., and O'Neill, L.A.J. (2020). The Role of HIF in Immunity and Inflammation. Cell Metabol. *32*, 524–536. https://doi.org/10.1016/J.CMET.2020.08.002.
21. Walter, W., Alonso-Herranz, L., Trappetti, V., Crespo, I., Ibberson, M., Cedenilla, M., Karaszewska, A., Núñez, V., Xenarios, I., Arroyo, A.G., et al. (2018). Deciphering the Dynamic Transcriptional and Post-transcriptional Networks of Macrophages in the Healthy Heart and after Myocardial Injury. Cell Rep. *23*, 622–636. https://doi.org/10.1016/j.celrep.2018.03.029.
22. Gorospe, M., Tominaga, K., Wu, X., Fähling, M., and Ivan, M. (2011). Post-Transcriptional Control of the Hypoxic Response by RNA-Binding Proteins and MicroRNAs. Front. Mol. Neurosci. *4*, 7. https://doi.org/10.3389/fnmol.2011.00007.
23. Zhang, J., Modi, Y., Yarovinsky, T., Yu, J., Collinge, M., Kyriakides, T., Zhu, Y., Sessa, W.C., Pardi, R., and Bender, J.R. (2012). Macrophage β2 Integrin–Mediated, HuR-Dependent Stabilization of Angiogenic Factor–Encoding mRNAs in Inflammatory Angiogenesis. Am. J. Pathol. *180*, 1751–1760. https://doi.org/10.1016/j.ajpath.2011.12.025.
24. Badawi, A., Biyanee, A., Nasrullah, U., Winslow, S., Schmid, T., Pfeilschifter, J., and Eberhardt, W. (2018). Inhibition of IRES-dependent translation of caspase-2 by HuR confers chemotherapeutic drug resistance in colon carcinoma cells. Oncotarget *9*, 18367–18385. https://doi.org/10.18632/ONCOTARGET.24840.
25. Durie, D., Hatzoglou, M., Chakraborty, P., and Holcik, M. (2013). HuR controls mitochondrial morphology through the regulation of Bcl xL translation. Translation *1*, e23980. https://doi.org/10.4161/TRLA.23980.
26. Kullmann, M., Göpfert, U., Siewe, B., and Hengst, L. (2002). ELAV/Hu proteins inhibit p27 translation via an IRES element in the p27 5′UTR. Genes Dev. *16*, 3087–3099. https://doi.org/10.1101/gad.248902.
27. Bhattacharyya, S.N., Habermacher, R., Martine, U., Closs, E.I., and Filipowicz, W. (2006). Relief of microRNA-Mediated Translational Repression in Human Cells Subjected to Stress. Cell *125*, 1111–1124. https://doi.org/10.1016/j.cell.2006.04.031.
28. Kundu, P., Fabian, M.R., Sonenberg, N., Bhattacharyya, S.N., and Filipowicz, W. (2012). HuR protein attenuates miRNA-mediated repression by promoting miRISC dissociation from the target RNA. Nucleic Acids Res. *40*, 5088–5100. https://doi.org/10.1093/nar/gks148.
29. Chang, S.-H., Lu, Y.-C., Li, X., Hsieh, W.-Y., Xiong, Y., Ghosh, M., Evans, T., Elemento, O., and Hla, T. (2013). Antagonistic Function of the RNA-binding Protein HuR and miR-200b in Post-transcriptional Regulation of Vascular Endothelial Growth Factor-A Expression and Angiogenesis. J. Biol. Chem. *288*, 4908–4921. https://doi.org/10.1074/jbc.M112.423871.
30. Shibata, N., Carlin, A.F., Spann, N.J., Saijo, K., Morello, C.S., McDonald, J.G., Romanoski, C.E., Maurya, M.R., Kaikkonen, M.U., Lam, M.T., et al. (2013). 25-Hydroxycholesterol activates the integrated stress response to reprogram transcription and translation in macrophages. J. Biol. Chem. *288*, 35812–35823. https://doi.org/10.1074/jbc.M113.519637.
31. Liu, J., Krautzberger, A.M., Sui, S.H., Hofmann, O.M., Chen, Y., Baetscher, M., Grgic, I., Kumar, S., Humphreys, B.D., Hide, W.A., and McMahon, A.P. (2014). Cell-specific translational profiling in acute kidney injury. J. Clin. Invest. *124*, 1242–1254. https://doi.org/10.1172/JCI72126.
32. Hofmeister, A., Thomaßen, M.C., Markert, S., Marquardt, A., Preußner, M., Rußwurm, M., Schermuly, R.T., Steinhoff, U., Gröne, H.J., Hoyer, J., et al. (2020). Development of a new macrophage-specific TRAP mouse (MacTRAP) and definition of the renal macrophage translational signature. Sci. Rep. *10*, 7519. https://doi.org/10.1038/s41598-020-63514-6.
33. Schott, J., Reitter, S., Philipp, J., Haneke, K., Schäfer, H., and Stoecklin, G. (2014). Translational Regulation of Specific mRNAs Controls Feedback Inhibition and Survival during Macrophage Activation. PLoS Genet. *10*, e1004368. https://doi.org/10.1371/journal.pgen.1004368.
34. Deng, L., Zhou, J.-F., Sellers, R.S., Li, J.-F., Nguyen, A.V., Wang, Y., Orlofsky, A., Liu, Q., Hume, D.A., Pollard, J.W., et al. (2010). A Novel Mouse Model of Inflammatory Bowel Disease Links Mammalian Target of Rapamycin-Dependent Hyperproliferation of Colonic Epithelium to Inflammation-Associated Tumorigenesis. Am. J. Pathol. *176*, 952–967. https://doi.org/10.2353/ajpath.2010.090622.
35. Heiman, M., Schaefer, A., Gong, S., Peterson, J.D., Day, M., Ramsey, K.E., Suárez-Fariñas, M., Schwarz, C., Stephan, D.A., Surmeier, D.J., et al. (2008). A Translational Profiling Approach for the Molecular Characterization of CNS Cell Types. Cell *135*, 738–748. https://doi.org/10.1016/j.cell.2008.10.028.
36. Zhou, P., Zhang, Y., Ma, Q., Gu, F., Day, D.S., He, A., Zhou, B., Li, J., Stevens, S.M., Romo, D., and Pu, W.T. (2013). Interrogating translational efficiency and lineage-specific transcriptomes using ribosome affinity purificationNo Title. Proc. Natl. Acad. Sci. USA *110*, 15395–15400. https://doi.org/10.1073/pnas.1304124110.
37. Megat, S., Ray, P.R., Moy, J.K., Lou, T.F., Barragán-Iglesias, P., Li, Y., Pradhan, G., Wanghzou, A., Ahmad, A., Burton, M.D., et al. (2019). Nociceptor Translational Profiling Reveals the Ragulator-Rag GTPase Complex as a Critical Generator of Neuropathic Pain. J. Neurosci. *39*, 393–411. https://doi.org/10.1523/JNEUROSCI.2661-18.2018.
38. Helmy, K., Halliday, J., Fomchenko, E., Setty, M., Pitter, K., Hafemeister, C., and Holland, E.C. (2012). Identification of global alteration of translational regulation in glioma in vivo. PLoS One *7*, e46965. https://doi.org/10.1371/JOURNAL.PONE.0046965.
39. Thomas, A., Lee, P.J., Dalton, J.E., Nomie, K.J., Stoica, L., Costa-Mattioli, M., Chang, P., Nuzhdin, S., Arbeitman, M.N., and Dierick, H.A. (2012). A versatile method for cell-specific profiling of translated mRNAs in

Drosophila. PLoS One *7*, e40276. https://doi.org/10.1371/JOURNAL.PONE.0040276.

40. Nectow, A.R., Moya, M.V., Ekstrand, M.I., Mousa, A., McGuire, K.L., Sferrazza, C.E., Field, B.C., Rabinowitz, G.S., Sawicka, K., Liang, Y., et al. (2017). Rapid Molecular Profiling of Defined Cell Types Using Viral TRAP. Cell Rep. *19*, 655–667. https://doi.org/10.1016/J.CELREP.2017.03.048.
41. Burkhart, R.A., Pineda, D.M., Chand, S.N., Romeo, C., Londin, E.R., Karoly, E.D., Cozzitorto, J.A., Rigoutsos, I., Yeo, C.J., Brody, J.R., and Winter, J.M. (2013). HuR is a post-transcriptional regulator of core metabolic enzymes in pancreatic cancer. RNA Biol. *10*, 1312–1323. https://doi.org/10.4161/rna.25274.
42. Fan, J., Ishmael, F.T., Fang, X., Myers, A., Cheadle, C., Huang, S.-K., Atasoy, U., Gorospe, M., and Stellato, C. (2011). Chemokine Transcripts as Targets of the RNA-Binding Protein HuR in Human Airway Epithelium. J. Immunol. *186*, 2482–2494. https://doi.org/10.4049/jimmunol.0903634.
43. Lin, G.L., Ting, H.J., Tseng, T.C., Juang, V., and Lo, Y.L. (2017). Modulation of the mRNA-binding protein HuR as a novel reversal mechanism of epirubicin-triggered multidrug resistance in colorectal cancer cells. PLoS One *12*, e0185625. https://doi.org/10.1371/journal.pone.0185625.
44. Stellos, K., Gatsiou, A., Stamatelopoulos, K., Perisic Matic, L., John, D., Lunella, F.F., Jaé, N., Rossbach, O., Amrhein, C., Sigala, F., et al. (2016). Adenosine-to-inosine RNA editing controls cathepsin S expression in atherosclerosis by enabling HuR-mediated post-transcriptional regulation. Nat. Med. *22*, 1140–1150. https://doi.org/10.1038/nm.4172.
45. Lu, Y.-C., Chang, S.-H., Hafner, M., Li, X., Tuschl, T., Elemento, O., and Hla, T. (2014). ELAVL1 Modulates Transcriptome-wide miRNA Binding in Murine Macrophages. Cell Rep. *9*, 2330–2343. https://doi.org/10.1016/j.celrep.2014.11.030.
46. Reines, B., Cheng, L.I., and Matzinger, P. (2009). Unexpected Regeneration in Middle-Aged Mice. Rejuvenation Res. *12*, 45–52. https://doi.org/10.1089/rej.2008.0792.
47. Zhang, Y., Strehin, I., Bedelbaeva, K., Gourevitch, D., Clark, L., Leferovich, J., Messersmith, P.B., and Heber-Katz, E. (2015). Drug-induced regeneration in adult mice. Sci. Transl. Med. *7*, 290ra92. https://doi.org/10.1126/scitranslmed.3010228.
48. Rajnoch, C., Ferguson, S., Metcalfe, A.D., Herrick, S.E., Willis, H.S., and Ferguson, M.W.J. (2003). Regeneration of the ear after wounding in different mouse strains is dependent on the severity of wound trauma. Dev. Dyn. *226*, 388–397. https://doi.org/10.1002/dvdy.10242.
49. Schott, J., Reitter, S., Lindner, D., Grosser, J., Bruer, M., Shenoy, A., Geiger, T., Mathes, A., Dobreva, G., and Stoecklin, G. (2021). Nascent Ribo-Seq measures ribosomal loading time and reveals kinetic impact on ribosome density. Nat. Methods *18*, 1068–1074. https://doi.org/10.1038/S41592-021-01250-Z.
50. Shi, Z., Fujii, K., Kovary, K.M., Genuth, N.R., Röst, H.L., Teruel, M.N., and Barna, M. (2017). Heterogeneous Ribosomes Preferentially Translate Distinct Subpools of mRNAs Genome-wide. Mol. Cell *67*, 71–83.e7. https://doi.org/10.1016/J.MOLCEL.2017.05.021.
51. Fernández-Silva, P., Enriquez, J.A., and Montoya, J. (2003). Replication and transcription of mammalian mitochondrial DNA. Exp. Physiol. *88*, 41–56. https://doi.org/10.1113/eph8802514.
52. Jian, B., Wang, D., Chen, D., Voss, J., Chaudry, I., and Raju, R. (2010). Hypoxia-induced alteration of mitochondrial genes in cardiomyocytes: Role of Bnip3 and Pdk1. Shock *34*, 169–175. https://doi.org/10.1097/SHK.0b013e3181cffe7d.
53. Chao, J., Wood, J.G., and Gonzalez, N.C. (2011). Alveolar macrophages initiate the systemic microvascular inflammatory response to alveolar hypoxia. Respir. Physiol. Neurobiol. *178*, 439–448. https://doi.org/10.1016/j.resp.2011.03.008.
54. Guilliams, M., De Kleer, I., Henri, S., Post, S., Vanhoutte, L., De Prijck, S., Deswarte, K., Malissen, B., Hammad, H., and Lambrecht, B.N. (2013). Alveolar macrophages develop from fetal monocytes that differentiate into long-lived cells in the first week of life via GM-CSF. J. Exp. Med. *210*, 1977–1992. https://doi.org/10.1084/jem.20131199.
55. Schneider, C., Nobs, S.P., Kurrer, M., Rehrauer, H., Thiele, C., and Kopf, M. (2014). Induction of the nuclear receptor PPAR-γ 3 by the cytokine GM-CSF is critical for the differentiation of fetal monocytes into alveolar macrophages. Nat. Immunol. *15*, 1026–1037. https://doi.org/10.1038/ni.3005.
56. Low, Q.E., Drugea, I.A., Duffner, L.A., Quinn, D.G., Cook, D.N., Rollins, B.J., Kovacs, E.J., and DiPietro, L.A. (2001). Wound healing in MIP-1alpha(-/-) and MCP-1(-/-) mice. Am. J. Pathol. *159*, 457–463.
57. Wood, S., Jayaraman, V., Huelsmann, E.J., Bonish, B., Burgad, D., Sivaramakrishnan, G., Qin, S., DiPietro, L.A., Zloza, A., Zhang, C., and Shafikhani, S.H. (2014). Pro-inflammatory chemokine CCL2 (MCP-1) promotes healing in diabetic wounds by restoring the macrophage response. PLoS One *9*, e91574. https://doi.org/10.1371/journal.pone.0091574.
58. Dewald, O., Zymek, P., Winkelmann, K., Koerting, A., Ren, G., Abou-Khamis, T., Michael, L.H., Rollins, B.J., Entman, M.L., and Frangogiannis, N.G. (2005). CCL2/monocyte chemoattractant protein-1 regulates inflammatory responses critical to healing myocardial infarcts. Circ. Res. *96*, 881–889. https://doi.org/10.1161/01.RES.0000163017.13772.3a.
59. Abtin, A., Jain, R., Mitchell, A.J., Roediger, B., Brzoska, A.J., Tikoo, S., Cheng, Q., Ng, L.G., Cavanagh, L.L., von Andrian, U.H., et al. (2014). Perivascular macrophages mediate neutrophil recruitment during bacterial skin infection. Nat. Immunol. *15*, 45–53. https://doi.org/10.1038/ni.2769.
60. Kolter, J., Feuerstein, R., Zeis, P., Hagemeyer, N., Paterson, N., d'Errico, P., Baasch, S., Amann, L., Masuda, T., Lösslein, A., et al. (2019). A Subset of Skin Macrophages Contributes to the Surveillance and Regeneration of Local Nerves. Immunity *50*, 1482–1497.e7. https://doi.org/10.1016/J.IMMUNI.2019.05.009.
61. Barreiro, O., Cibrian, D., Clemente, C., Alvarez, D., Moreno, V., Valiente, Í., Bernad, A., Vestweber, D., Arroyo, A.G., Martín, P., et al. (2016). Pivotal role for skin transendothelial radio-resistant anti-inflammatory macrophages in tissue repair. Elife *5*, e15251. https://doi.org/10.7554/eLife.15251.
62. Pertea, M., Kim, D., Pertea, G.M., Leek, J.T., and Salzberg, S.L. (2016). Transcript-level expression analysis of RNA-seq experiments with HISAT, StringTie and Ballgown. Nat. Protoc. *11*, 1650–1667. https://doi.org/10.1038/nprot.2016.095.
63. Love, M.I., Huber, W., and Anders, S. (2014). Moderated estimation of fold change and dispersion for RNA-seq data with DESeq2. Genome Biol. *15*, 550. https://doi.org/10.1186/s13059-014-0550-8.
64. Davies, J.Q., and Gordon, S. (2005). Isolation and culture of murine macrophages. Methods Mol. Biol. *290*, 91–103. https://doi.org/10.1385/1-59259-838-2:091.
65. Heiman, M., Kulicke, R., Fenster, R.J., Greengard, P., and Heintz, N. (2014). Cell type-specific mRNA purification by translating ribosome affinity purification (TRAP). Nat. Protoc. *9*, 1282–1291. https://doi.org/10.1038/nprot.2014.085.
66. Hulsen, T., de Vlieg, J., and Alkema, W. (2008). BioVenn - a web application for the comparison and visualization of biological lists using area-proportional Venn diagrams. BMC Genom. *9*, 488.

STAR★METHODS

KEY RESOURCES TABLE

REAGENT or RESOURCE	SOURCE	IDENTIFIER
Antibodies		
Pacific Blue™ anti-CD11b (Rat, 1:50)	BioLegend	Cat # 101224, RRID: AB_755986
Alexa Fluor® 647 anti-F4/80 (Rat, 1:100)	BioLegend	Cat # 123122, RRID: AB_893480
Anti-HuR 3A2 (Mouse, 1:50)	Santa Cruz	Cat # sc-5261, RRID: AB_627770
PE anti-mouse CD88 (C5aR) antibody	BioLegend	Cat # 135805, RRID:AB_2067285
PE anti-mouse Ly-6A/E	BioLegend	Cat # 108107, RRID:AB_313344
Anti-PGK1 Antibody (14)	Santa Cruz	Cat # sc-130335, RRID:AB_2268001
Anti-PGK1 Antibody (clone W18295A)	BioLegend	Cat # 603251, RRID:AB_2910481
Anti-Actin Antibody (C-2)	Santa Cruz	Cat # sc-8432, RRID:AB_626630
Anti-Actin Antibody (rabbit mAb clone ARC5115-02)	ABclonal	Cat # AC048
Alexa Fluor® 680 donkey anti-rabbit	ThermoFisher	Cat # A10043
Alexa Fluor® 680 donkey anti-mouse	ThermoFisher	Cat # A10038
Alexa Fluor® 680 goat anti-rat	ThermoFisher	Cat # A21096
IgG2b, κ Isotype control (Rat, 1:100)	BioLegend	Cat # 400627, RRID: AB_493561
IgG2a, κ Isotype control (Rat, 1:100)	BioLegend	Cat # 400526 RRID:AB_2864284
Chemicals, peptides, and recombinant proteins		
RPMI 1640 Medium	ThermoFisher	Cat # 11875119
HEPES solution	Millipore Sigma	Cat # H4034
2-mercaptoethanol	Millipore Sigma	Cat # M3148
1,2-diheptanoyl-sn-glycero-phosphocholine (DHPC)	Avanti Polar Lipids	Cat # 850306P
IGEPAL CA-630	Millipore Sigma	Cat # I3021
Cycloheximide	Millipore Sigma	Cat # C7698
cOmplete™, Mini, EDTA-free Protease Inhibitor Cocktail	Millipore Sigma	Cat # 11836170001
RNAseOUT™ Recombinant Ribonuclease Inhibitor	Life Technologies	Cat # 10777019
GFP-TRAP_MA	Chromotek	Cat # gtma, RRID:AB_2631358
Binding control	Chromotek	Cat # bmab, RRID:AB_2827548
Stainless Steel Beads 5 mm	QIAGEN	Cat # 69989
SureBeads™ Protein G Magnetic Beads 1614023	Bio-Rad	Cat # 1614023
Dimethyloxaloylglycine (DMOG)	Cayman Chemicals	Cat # 71210
Dimethylsulfoxide (DMSO)	Millipore Sigma	Cat # D2650
Precision Plus Protein Dual Color Standards	BioRad	Cat # 1610374
Intercept® Blocking Buffer	LI-COR	Cat # 927-70001
Blocking buffer for fluorescent western protein	Rockland	Cat # MB-070
Critical commercial assays		
Direct-Zol RNA MiniPrep Plus	Zymo Research	Cat # R2073
iScript cDNA Synthesis Kit	BioRad	Cat # 1708891
Zenon™ Alexa Fluor™ Mouse IgG1 Labeling Kit	ThermoFisher	Cat # Z25008, RRID: AB_2736959

(*Continued on next page*)

Continued

REAGENT or RESOURCE	SOURCE	IDENTIFIER
ELISA MAX™ Deluxe Set for Mouse MCP-1/Ccl2	BioLegend	Cat # 432704
FastStart Universal SYBR Green Master (Rox)	Millipore Sigma	Cat # 04913850001
Deposited data		
BMDM TRAP-sequencing	This paper	GEO: GSE196517
FLDM TRAP-sequencing	This paper	GEO: GSE196966
Tools		
Disposable biopsy punch 2-mm and 6-mm	Integra Life Sciences	33-31 and 33-36
Experimental models: Cell lines		
MH-S macrophage cell line	ATCC	CRL-2019
Experimental models: Organisms/strains		
Cfs1r-iCre mice CFVB-Tg(Csf1r-icre)1Jwp/J	The Jackson Laboratory	Strain # 021024
LysMcre mice B6;129S4-B6.129P2-Lyz2tm1(cre)Ifo/J	The Jackson Laboratory	Strain #004781
EGFP-L10a mice B6;129S4-Gt(ROSA) 26Sortm9(EGFP/Rpl10a)Amc/J	The Jackson Laboratory	Strain #024750
$HuR^{fl/fl}$ mice Elavl1tm1.1Bndr	Zhang et al.[23]PMID: 22322302	MGI:5316082
Oligonucleotides		
Please see Table S3.		
Software and algorithms		
HiSAT2 and Ballgown	Pertea et al.[62]	https://daehwankimlab.github.io/hisat2/, RRID: SCR_015530
DESeq2	Love et al.[63]	https://bioconductor.org/packages/release/bioc/html/DESeq2.html, RRID: SCR_015687
FlowJo V7.6.5	FlowJo, LLC.	https://www.flowjo.com/solutions/flowjo, RRID: SCR_008520
GraphPad Prism version 9	GraphPad Software, Inc.	https://www.graphpad.com, RRID: SCR_002798
Ingenuity Pathway Analysis	QIAGEN Bioinformatics	http://www.ingenuity.com/products/pathways_analysis.html, RRID: SCR_008653

RESOURCE AVAILABILITY

Lead contact

Further information and reasonable requests for resources and reagents should be directed to the lead contact, Dr. Jeffrey Bender (jeffrey.bender@yale.edu).

Materials availability

This study did not generate any unique materials.

Data and code availability

This study did not generate any new code. RNA-seq data have been deposited to GEO with the identifiers listed below. Any additional information required to reanalyze the data reported in this paper is available from the lead contact upon request.

EXPERIMENTAL MODEL AND STUDY PARTICIPANT DETAILS

Animals, macrophage differentiation, and ear punch hole injury model

We purchased $Csf1r^{iCre}$ (FVB-Tg(Csf1r-icre)1Jwp/J, stock # 021024), LysMcre (B6;129S4-B6.129P2-Lyz2tm1(cre)Ifo/J, Strain #004781) and $Rosa26^{EGFP:L10a}$ (B6;129S4-Gt(ROSA)26Sortm9(EGFP/Rpl10a)Amc/J, stock # 024750) mice from the Jackson Laboratory and backcrossed

them to C57BL/6J genetic background to a total of 6 generations prior to establishing the cross of mice homozygous for both Csf1r^{iCre} and Rosa26$^{EGFP:L10a}$ transgenes. To delete HuR in differentiated macrophages, we crossed Csf1r^{iCre}Rosa26$^{EGFP:L10a}$ mice to HuR$^{fl/fl}$ mice that were previously generated and maintained on C57BL/6J genetic background in our laboratory.[23] We used the resulting HuR$^{fl/fl}$Csf1r^{iCre}Rosa26$^{EGFP:L10a}$ mice (8-12 week-old) to isolate HuR-KO BMDM or to establish timed breeding for isolation of embryonic HuR-KO FLDM. HuR$^{+/fl}$Csf1r^{iCre}Rosa26$^{EGFP:L10a}$ mice were used for control BMDM and HuR$^{+/+}$Csf1r^{iCre}Rosa26$^{EGFP:L10a}$ mice were used for control FLDM. We used LysMcre cross to HuR$^{fl/fl}$ mice to achieving myeloid cell-specific HuR deletion as previously described.[23] All breeder mice and mice used for this study were routinely genotyped using protocols from the Jackson Laboratory or prior publication.[23] When possible, we used female and male animals at equal ratio for BMDM isolations and ear punch injury study to minimize bias to one sex. All animal procedures were approved by Yale University IACUC.

We used previously established protocol for *in vitro* differentiation of BMDM from femur and tibia bones from 8-12 week-old mice that were euthanized by cervical dislocation following anesthesia with isoflurane.[64] We differentiated FLDM from single cell suspension obtained from E14.5 embryonic livers. We confirmed the date of conception (D0) by identification of vaginal mucus plug in dam and tracked progression of successful pregnancy by tracking changes in body weights. Dams were anesthetized by isoflurane and euthanized by cervical dislocation. Embryonic age was confirmed by counting somite pairs in embryos after dissection. Fetal livers were dissected and pooled from one litter into 10 ml of PBS supplemented with 10% FBS, mechanically dissociated by pipetting up and down vigorously, before being filtered through a 40-μM cell strainer into a 50-mL conical tube and washed by centrifugation (1500 rpm at 4°C for 5 minutes). To remover the contaminating red blood cells, we resuspended the pellets in 10 mL of ACK lysis buffer (0.15 mM NH4Cl, 1 mM KHCO3, 0.1 mM EDTA) and incubated for 5 minutes prior to washing in 20 mL of FBS-supplemented PBS. Differentiation of BMDM and FLDM was started from 3.5*10^6 cells/plate in 100-mm non-tissue culture treated plastic Petri dishes in 10 ml of RPMI-1640 culture media supplemented with 10% FBS, 2mM L-glutamine, 100 U/ml penicillin/streptomycin, 10 mM HEPES, 50 μM 2-mercaptoethanol and 33% L-cell conditioned medium and proceeded for 6 days under identical conditions. Fresh culture medium was added at day 3. Non-adherent cells were removed with change of medium at day 6. Macrophage differentiation and L10a-EGFP expression were confirmed by observation of adherent cells and EGFP fluorescence using inverted microscope (Leica DM IRB) equipped with DC350FX camera (Leica) and ImagePro software as well as by expression of macrophage-specific marker (F4/80) using flow cytometry.

To model tissue injury and repair, we anesthetized animals with isoflurane, placed them into a supine position and punched through the middle of the left ear using a sterile disposable 2-mm ear punch. We photographed the wounded ears from the rear of the anesthetized animals with a backdrop of a ruler in the same plane as the ear immediately and on days 4, 7, 15, and 35 after the injury and measured the open wound area using ImageJ software. Using a separate cohort of mice, we collected the tissue surrounding the open would and the control tissue from contralateral intact ear from wild-type and myeloid HuR-KO mice euthanized on day 4 after injury. The collected tissues were snap-frozen in liquid nitrogen and stored at −70°C until total RNA extraction into 300 μl TRI-Reagent (Zymo Research) or protein extraction into 300 μl RIPA lysis buffer with 5-mm stainless still beads and TissueLyzer. The RNA samples were used for qRT-PCR, while cleared protein samples were used to measure Ccl2 concentration by ELISA.

METHOD DETAILS

Hypoxia exposure

On day 7 of culture, cells were placed in a hypoxic modular incubator chamber (Billups-Rothenberg). Petri dishes containing cultured cells were placed in the chamber. A ring clamp was used create an air-tight seal along the O-ring of the chamber. The tubing of the outlets was unclamped and connected to a tank containing a mixture of 1% O_2 and 5% CO_2 balanced with nitrogen (Airgas East). The chamber was gassed for 10-minutes before the tubing was disconnected from the tank and outlets quickly clamped. The hypoxia chamber was subsequently placed in a 37°C incubator. Normoxic controls were concurrently incubated at 37°C. The duration of hypoxia was 18 h and the chamber was re-gassed at 4-hour intervals.

Translating ribosome affinity purification (TRAP) and RNA isolation

We obtained the total and translated RNA pools using previously published protocol with minor modifications.[65] At the conclusion of the 18-hour incubation under normoxia or hypoxia conditions, cells were treated with 100 μg/ml cycloheximide for 30 min, washed with ice-cold PBS containing 100 μg/ml cycloheximide, and lysed in ice-cold lysis buffer (150 mM KCl, 10 mM $MgCl_2$, 20 mM HEPES, 1% NP-40, 0.5 mM DTT, 100 μg/ml cycloheximide) supplemented with cOmplete™ Protease and Phosphatase inhibitors (Roche), and 2000 U/ml RNaseOUT™ (ThermoFisher). Scraped lysates were precleared by centrifugation at 2000 g for 10 min at 4°C and the microsomal membranes were solubilized by incubation in the presence of 30 mM 1,2-diheptanoyl-sn-glycero-phosphocholine (DHPC, Avanti Polar Lipids) for 5 min at 4°C. Insoluble fraction was removed by centrifugation at 20,000 g for 10 min at 4°C. The resulting lysates were used to isolate total RNA using Direct-Zol RNA MiniPrep Plus (Zymo Research) or to affinity purify ribosomes with translated RNA using GFP-TRAP beads (magnetic agarose beads coated with Alpaca anti-GFP VHH antibody, Chromotek). Incubation with the GFP-TRAP beads proceeded for 3 h at 4°C with gentle end-over-end mixing in a tube rotator and was followed by three washes with high salt buffer (350 mM KCl, 10 mM $MgCl_2$, 20 mM HEPES, 1% NP-40, 0.5 mM DTT, 100 μg/ml cycloheximide). Translated RNA was eluted from the beads by incubation in TRIZOL and isolated using Direct-Zol RNA MiniPrep Plus (Zymo Research).

RNA aliquots were stored at −70°C and only thawed once to minimize RNA degradation. RNA Quality Control analysis was performed using Agilent TapeStation 2200. Only samples with RNA Integrity Numbers >7 were used for subsequent analyses.

Immunoblotting

BMDM and FLDM were differentiated and exposed to hypoxia as described above, rinsed with ice-cold PBS and lysed in 400 μl of lysis buffer containing 1% Igepal (Sigma) and complete protease inhibitors. Scraped lysates were precleared by centrifugation at 14,000 g for 10 min at 4°C. We separated proteins in 4–20% precast gradient gels (Bio-Rad) and transferred them onto nitrocellulose membrane. After 1 h blocking with the blocking buffer (Rockland), we probed the membranes sequentially with mouse anti-HuR (clone 3A2) and anti-actin primary antibodies (both from SantaCruz) and with goat anti-mouse AlexaFluor™ -680-conjugated secondary antibodies (ThermoFisher). We scanned the blots with LICOR Odyssey system and analyzed the intensity of the bands with ImageStudio Lite software version 5.2.

HuR-RNA immunoprecipitation (IP)

Macrophage cell line MH-S (originally derived from a male mouse) was grown in RPMI-1640 medium supplemented with 10% FBS, 100 U/ml penicillin/streptomycin and 50 μM 2-mercaptoethanol. Following a wash in PBS by centrifugation, $40x10^6$ cells were lysed on ice in lysis buffer containing 1% Igepal, cOmplete™ Protease and Phosphatase inhibitors, and 2000 U/ml RNaseOUT. Scraped lysates were precleared by centrifugation at 14,000 g for 10 min at 4°C and divided into input (10% of the volume), HuR IP (45%), and isotype control IP (45%). Corresponding antibodies (anti-HuR clone 3A2 or isotype control IgG1κ) were added to the IP reactions (4 μg/ml). After incubation at 4°C with rotation for 2 h, washed SureBeads™ Protein G magnetic beads were added to the IP reactions (50 μl) and incubation continued with rotation at 4°C for additional 1 h. Beads were washed 4 times with NT2 buffer (50 mM Tris-HCl pH 7.4, 150 mM NaCl, 1 mM $MgCl_2$,0.05% Igepal). Input, which was marinated on ice for the duration of the immunoprecipitation, and the IP reactions were used to isolate RNA and qRT-PCR.

qRT-PCR

Between 100 and 200 ng of total RNA (measured by NanoDrop) was used to generate cDNA with iScript cDNA Supermix kit (Bio-Rad). The resulting cDNA was diluted 10-fold and used for qPCR analyses using custom-designed primers and FastStart SYBR Green Master mix (Roche/SigmaAldrich) in CFX96 Real-Time PCR detection system (BioRad). Meltcurve analyses, no reverse-transcriptase and no template controls were used to exclude primer-dimers and non-specific amplification from residual genomic DNA. The results were quantified using ΔCq method, normalized to reference transcripts (Hprt), and expressed as relative expression or fold change to control samples.

Flow cytometry analyses and measurements of mRNA translation efficiency

Adherent macrophages were washed with PBS and incubated in 10 mM EDTA in PBS for 10 min at 4°C to bring them into suspension by pipetting. Cells were washed with FACS buffer (3% FBS, 0.1% sodium azide in PBS) prior to blocking the Fc receptors with Fc Block™ (BD Biosciences) and surface staining with conjugated antibodies (CD11b-Pacific Blue™, F4/80-AlexaFluor™ 647, Ly6e-PE, CD88-PE, and corresponding isotype controls) with antibodies on ice for 30 min. The cells were washed 3 times with cold FACS buffer prior to acquisition or fixation. For intracellular staining, the cells were fixed and permeabilized with eBioscience™ Foxp3 Transcription Factor Staining Buffer set and incubated with anti-PGK antibody or IgG1κ isotype control labeled with AlexaFluor™ 647 using Zenon™ IgG1 kit (ThermoFisher). Permeabilization buffer was used for 3 washes prior to acquisition. Yale Flow Cytometry Core BD LSR II or BD LSR Fortessa with FACS Diva software were used to acquire fluorescence signal for single cells based on gating for forward and side scatter. Subsequent analyses of cell populations were performed using FlowJo software (v. 7.6.5).

For assessment of mRNA translation efficiency, parallel cultures of macrophages were treated with 10 μg/ml cycloheximide (CHX) or vehicle control (0.1% DMSO) prior to exposure to hypoxia. Cells were harvested as described above. One half of the cell sample was used for FACS analyses and the other half was used for RNA isolation and qRT-PCR. Translation rate for each target was calculated as follows: $(MFI_{control}-MFI_{CHX})/MFI_{control}$, where MFI is the geometric mean fluorescence intensity in the vehicle control or CHX-treated samples; in both cases after subtraction of the background MFI from the isotype control. Translation efficiency was calculated by dividing the translation rate by the relative abundance of the corresponding mRNA, measured by qRT-PCR. A scaling factor was applied for each target to maintain the scale similar to the TRAP RNASeq data at normoxia.

QUANTIFICATION AND STATISTICAL ANALYSIS

RNA-seq analyses

Total and translated RNA pools were used to prepare poly(A)-enriched cDNA libraries using standard protocol for BMDM and low input protocol for FLDM. Multiplex (8 samples/lane) paired-end (75 bp) sequencing was carried out using Illumina HiSeq 2500 at Yale Center for Genome Analyses. Raw sequencing data were trimmed for quality and aligned to the *Mus musculus* reference genome GRCm38 using HiSAT. The alignments were processed using Ballgown, and per-gene counts were obtained. The raw counts were initially processed using DESeq2 and R.

Subsequent analyses used Transcripts Per kilobase Million (TPM) as a measure of mRNA abundance in total and translated poly(A) samples and Log2 fold change (Log2FC) to determine the effects of hypoxia within the related samples. Log2FC were compared using multiple *t* tests with false-discovery rate (FDR) approach determined by the two-stage step-up method of Benjamini, Krieger and Yekutieli to identify transcripts that significantly increased or decreased in response to hypoxia based on desired FDR Q = 1%. Statistical analyses of the samples derived from BMDM and FLDM were performed separately. Only the protein coding transcripts showing statistically significant fold change (Log2FC > 0.263 or Log2FC < −0.263) in response to hypoxia were used for subsequent analyses. The resulting lists of transcripts differentially expressed or translated in response to hypoxia were displayed and analyzed using BioVenn web application[66] and Ingenuity Pathway Analyses (QIAGEN).